AP-E301592 (1)

A CLUTTER MODEL FOR SPACE BASED RADAR

Carl J. Lauer
Mission Research Corporation
P.O. Drawer 719
Santa Barbara , California 93102

1 November 1983

Technical Report

APPROVED FOR PUBLIC RELEASE;
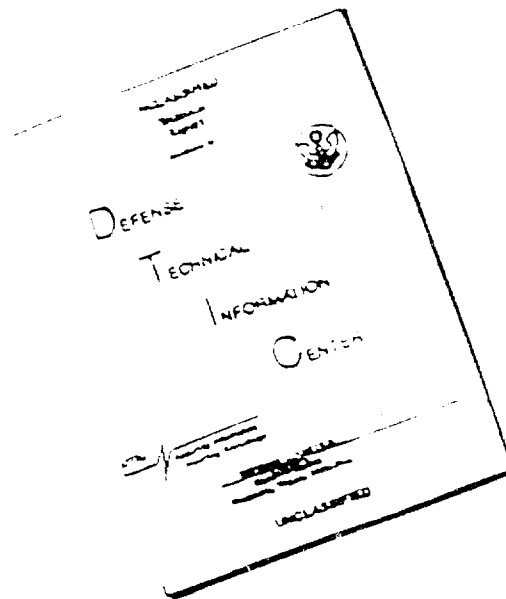DISTRIBUTION UNLIMITED.

Prepared for
Director
DEFENSE NUCLEAR AGENCY
Washington, DC 20305

DTIC
ELECTE
FEB 19 1985
S   D
          B

DTIC FILE COPY

84 12 19 032

DISCLAIMER NOTICE

THIS DOCUMENT IS BEST QUALITY AVAILABLE. THE COPY FURNISHED TO DTIC CONTAINED A SIGNIFICANT NUMBER OF PAGES WHICH DO NOT REPRODUCE LEGIBLY.

REPORT DOCUMENTATION PAGE	READ INSTRUCTIONS BEFORE COMPLETING FORM

1. REPORT NUMBER	2. GOVT ACCESSION NO.	3. RECIPIENT'S CATALOG NUMBER
DNA-TR-83-35	AD-A150 279	

4. TITLE (and Subtitle)	5. TYPE OF REPORT & PERIOD COVERED
A CLUTTER MODEL FOR SPACE BASED RADAR	Technical Report
	6. PERFORMING ORG. REPORT NUMBER MRC-N-602

7. AUTHOR(s)	8. CONTRACT OR GRANT NUMBER(s)
Carl J. Lauer	DNA 001-83-C-0021

9. PERFORMING ORGANIZATION NAME AND ADDRESS	10. PROGRAM ELEMENT, PROJECT, TASK AREA & WORK UNIT NUMBERS
Mission Research Corporation PO Drawer 719 Santa Barbara, CA 93102	Task S99QMXBA-00001

11. CONTROLLING OFFICE NAME AND ADDRESS	12. REPORT DATE
Director Defense Nuclear Agency Washington, DC 20305	1 November 1983
	13. NUMBER OF PAGES 58

14. MONITORING AGENCY NAME & ADDRESS(if different from Controlling Office)	15. SECURITY CLASS (of this report)
	UNCLASSIFIED
	15a. DECLASSIFICATION/DOWNGRADING SCHEDULE N/A since UNCLASSIFIED

16. DISTRIBUTION STATEMENT (of this Report)

Approved for public release, distribution is unlimited.

17. DISTRIBUTION STATEMENT (of the abstract entered in Block 20, if different from Report)

19. KEY WORDS (Continue on reverse side if necessary and identify by block number)

Space Based Radar
Pulse Doppler
Ground Clutter

20. ABSTRACT (Continue on reverse side if necessary and identify by block number)
A clutter model for a pulse doppler space based radar simulation is described. Ground clutter is represented as a random process with mean power, mean doppler, and doppler spread determined from experimental measurements and from physical and geometrical quantities pertinent to the radar location, look angle, beam pattern, etc. The above three quantities are used to define the clutter spectrum observed at a given radar range gate, and a statistical signal generation technique is employed to generate a realization or sample of the instantaneous clutter signal observed.

DD FORM 1473 JAN 73 EDITION OF 1 NOV 65 IS OBSOLETE

PREFACE

Various aspects of this work were improved by helpful
discussions with Dr. Dennis L. Knepp and Mr. Brian P.
O'Shaughnessy of Mission Research Corporation.

1

TABLE OF CONTENTS

LIST OF ILLUSTRATIONS

4

SECTION 1

INTRODUCTION

A space based radar (SBR) that must search for and track targets moving close to the earth's surface must be designed to discriminate between these targets and radar clutter caused by the undesired signal returned from the earth. For targets that are very close to the earth, clutter and target returns can appear at the same range in the radar receiver. If this condition occurs, an MTI or a pulse doppler radar may be used to discriminate on the basis of doppler measurements. However, since the clutter return usually exceeds the target return by many orders of magnitude, care must be taken during the coherent processing to avoid effects such as aliasing and spectral leakage. Thus an accurate simulation of a space based radar must include an accurate model of land and sea clutter in order to evaluate the performance of different coherent processing techniques.

The purpose of this report is to describe a clutter model intended for implementation in a pulse doppler tracking radar simulation. A standard approach to clutter modeling (e.g. Reference 1) involves division of the ground area illuminated by the radar antenna into a number of cells. A discrete scatterer of known cross section, amplitude, doppler frequency and location is assigned to each cell to represent all returns from a differential area element. These discrete scatterers or clutter targets then enter a receiver simulation in the same way as returns from any other target (e.g. an aircraft). Advantages of this approach are that it is straightforward to implement and that it can be made increasingly accurate by using a greater number of cells. Unfortunately, because of the large area illuminated by an SBR, the large doppler extent, and the

resolution required, an unacceptably high number of clutter targets would be required.

Here a second approach has been adopted. This technique consists of modeling the clutter as a random process with mean power, mean doppler, and doppler spread determined from experimental measurements and from physical and geometrical quantities pertinent to the radar location, look angle, beam pattern, etc. The above three quantities are used to define the clutter spectrum observed at a given radar range gate, and a statistical signal generation technique is employed to generate a realization or sample function of the instantaneous clutter signal observed. This method permits simple interpretation of results and reduces simulation running time since only one target requires processing. The accuracy can be increased with the level of detail of the analytic clutter model.

SECTION 2

MODELING APPROACH

The goal of this work is to provide a clutter model appropriate
to a high resolution pulse doppler SBR. It is desired that the model
provide realizations or sample functions of the clutter video; that is,
the model should provide the clutter voltage and phase as a function of
range gate for all the pulses of a coherent pulse train. It is convenient
to separate the clutter signal returned through the main beam of the
antenna from that returned through the antenna sidelobes. The footprint
on the earth's surface defined by the 3 dB contour of the two-way antenna
pattern defines the area that contributes to the main beam signal; the
remaining area contributes to the sidelobe signal. Of course the
illuminated areas are further limited by range gating, and ambiguous range
returns must be accounted for. These effects are discussed in Section 4.

Because of the fortunate statistics of the clutter signal
observed by the radar, it is possible to utilize a simple Fourier
transform technique to generate realizations of the clutter video signal
observed at a range gate. Given an analytical or numerical description of
the mean clutter spectrum, in this technique a realization or sample
function of the clutter voltage is obtained by taking the discrete Fourier
transform of a specified random sequence. The necessary mathematics and
justification of this method are fully described in the Appendix. An
essential assumption is that the quadrature components of the clutter
voltage are uncorrelated Gaussian variates.

In order to simplify the sea clutter model developed herein,
it is assumed that the clutter power spectrum is well represented as a

7

Gaussian in frequency whose power and spectral spread may be computed on the basis of the SBR-earth geometry with consideration of the illumination and receiving pattern of the SBR antenna.

The clutter return has been found to be uncorrelated from one burst waveform to another when the RF carrier frequency is changed by at least the reciprical of the pulse width[2]. Since the normal mode of operation of an SBR is to change radar frequency between pulse trains, this decorrelation property is retained here in the generation of the clutter for successive pulse trains.

In practice, the mean clutter spectrum is obtained in the simulation at the start of each dwell or coherent pulse train. It is assumed that the geometry does not change during the coherent integration time (dwell duration) so that the clutter spectrum is constant during this period. For each dwell a sequence of numbers is drawn from a random number generator and a realization of the clutter signal is generated as described in the Appendix. Succeeding dwells are assumed to utilize a different radar frequency and thus require a new sequence of random numbers to generate independent clutter signals. Thus, for each coherent pulse train, the clutter signal at a particular range bin is determined using a statistical signal generation technique.

The above discussion applies to clutter observed through the antenna main beam as well as to clutter that enters the receiver through the antenna sidelobes. In the case of sidelobe clutter, it will be shown that a flat power spectrum is appropriate and only the clutter power is required. In addition, simpler signal generation techniques are feasible that do not require Fourier tranforms.

Our discussion thus far has focused on modeling the signal in a single range bin. When range tracking is performed, the signals in

8

several adjacent bins must be modeled and it is important to include the effect of bin-to-bin correlation. For sea clutter, experimental data reported over a wide range of pulse widths and carrier frequencies demonstrates that the clutter returns decorrelate over a range displacement of about one pulse length, when the range is measured in units of delay . This is understood by realizing that since many independent scatterers contribute to sea clutter returns, the correlation for two returns separated in range is approximately equal to the fraction of illuminated ground area which is shared by the returns. For rectangular pulses with low sidelobes, the correlation is triangular and goes to zero at a range displacement equal to a pulse length. Thus the sea clutter returns will be uncorrelated for range bins separated by more than a (compressed) pulse length.

In general, the effects of ambient refraction are unimportant for the clutter model described here. Even for low altitude orbits the path length over which refraction occurs comprises a very small fraction of the total satellite to earth path. Thus, the fractional change in radar range is very small and will not significantly impact calculation of the illuminated areas or the radar range equation. The largest effect is an increase of clutter reflectivities that occurs with increasing grazing angle. This effect is important only for grazing angles less than a few degrees; fortunately this range is outside that currently under consideration for SBR operation. If SBR operation at very small grazing angles is to be included here, the calculation of grazing angles must be modified to include deviations caused by refraction.

Signal doppler effects are dependent on the earth's surface rotational velocity and this has been included in our formulation. First, for the sake of simplicity, we treat the doppler effects under the assumption of a non-rotating earth. Later, the approach is extended to the case of a rotating earth. In this regard the radar look angles are measured relative to the satellite's velocity vector which lies in the horizontal

plane as shown in Figure 1. In conformance with the later discussion which includes the effects of rotation of the earth and of vertical satellite motion, the elevation angle (EL) is negative for a downward looking line-of-sight (LOS).

A pulse doppler radar is able to mitigate the effects of clutter by separating target and clutter in the doppler frequency domain through the use of a large number of coherent pulses repeated in time at a high pulse repetition frequency (PRF). An increase in the PRF gives an increase in the total doppler bandwidth surveyed. An increase in the number of pulses increases the power as well as the doppler resolution. Pulse amplitude weighting on receive is utilized to suppress doppler side-lobes associated with the coherent processing. The effect of a particular clutter target depends upon the radar velocity, wavelength and the angle of the clutter from the antenna boresight. Since returns from clutter are weighted by the antenna pattern, improvement in clutter rejection can be obtained by narrowing the antenna beam. This technique not only realizes less overall clutter power but also decreases the spectral spread of the clutter contribution by selectively removing returns from high off-axis angles.

A quadratic phase shift applied on a pulse-to-pulse basis can be implemented in order to mitigate the spread in the main beam clutter signal due to ambiguous range returns (Reference 2). Quadratic phase shift processing (QPSP) is discussed in detail in Section 4. Improvement in clutter rejection can be large and depends upon the SBR look angle and the relative importance of platform motion on the clutter spectral width.

Another technique for reducing platform motion caused doppler spread which is not investigated here is the use of displaced phase center antennas (Skolnik, Reference 4; Knepp and Dana, Reference 5).

10
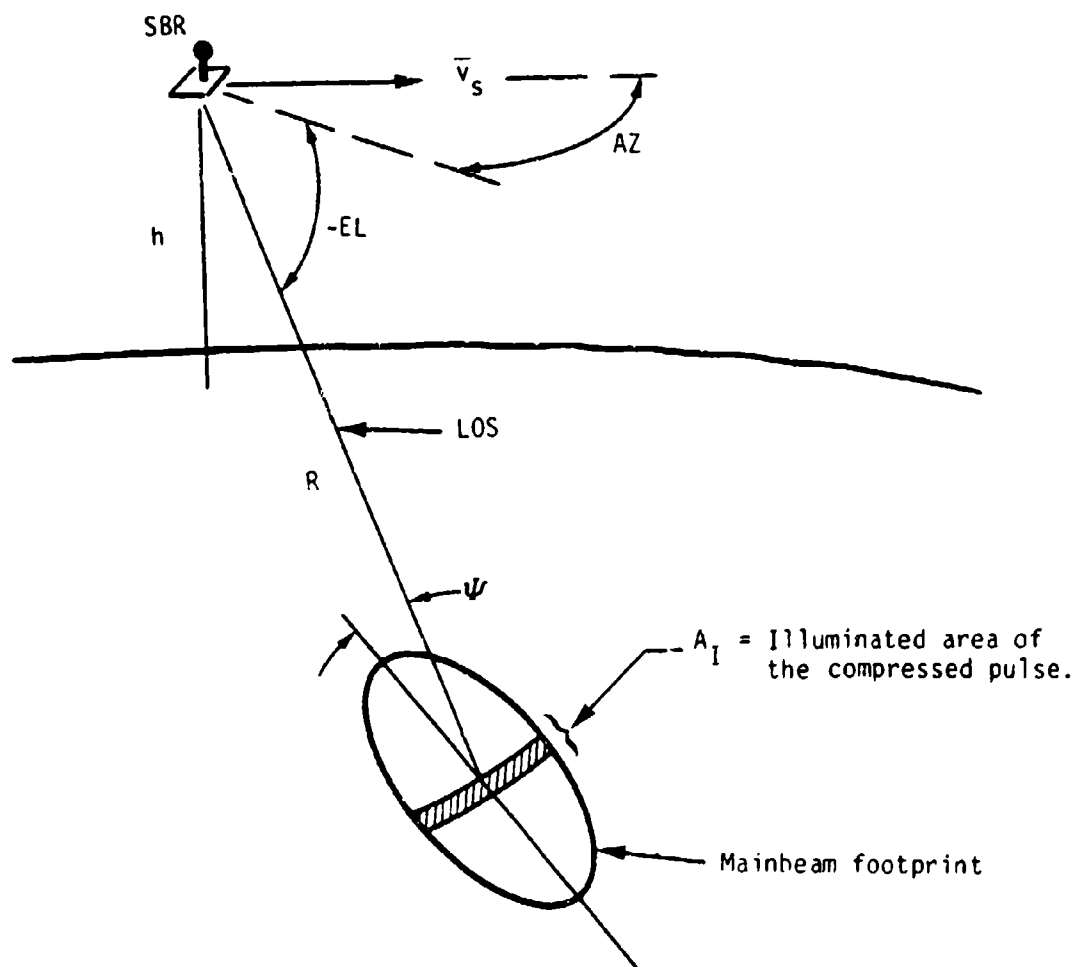
Figure 1. Clutter calculation geometry.

11

SECTION 3

SEA CLUTTER REFLECTIVITY MODEL

Sea clutter is the radar echo received as a result of reflections from the sea's surface. The effective radar cross section (RCS) of the sea echo may be predicted by taking the product of the sea reflectivity and the area that contributes to the echo strength. Sea clutter reflectivity is usually reported in terms of the parameter σ_0, the mean radar cross section per unit area of illuminated surface. Thus, a value of $\sigma_0 = -30$ dB corresponds to an average reflectivity of 10^{-3}. σ_0 is a function of grazing angle (defined as the angle between the tangent to the surface and the radar LOS), polarization, frequency, and sea state.

Because of the wide range of SBR look angles of interest, a model of σ_0 over the range of grazing angles from a few degrees up to normal incidence is required. Data at high grazing angle is necessary to estimate the sidelobe altitude return, although the SBR main beam would be overwhelmed by clutter at grazing angles greater than 50 or 60 degrees. The model we have determined for σ_0 is shown in Figure 2 as a function of grazing angle at L-band (1.5 GHz). Two curves are shown, the high wind (HW) and low wind (LW) models, with the difference in the two representing the effect of heavy and light seas, respectively. The equations for this model are

$$\sigma_0 = 7.0 \cdot 10^{\cdot 6}\psi^{2 \cdot 01} + 0.841 \exp\left\{-(\pi/2-\psi)^2/.0247\right\}; \text{ HW} \quad (1)$$

$$\sigma_0 = 3.6 \cdot 10^{-6}\psi^{2 \cdot 22} + 2.810 \exp\left\{-(\pi/2-\psi)^2/.0149\right\}; \text{ LW} \quad (2)$$

where ψ is the grazing angle in radians. The first terms in the above are the high wind, low wind models of Tomlinson[6] evaluated at L-band. We have
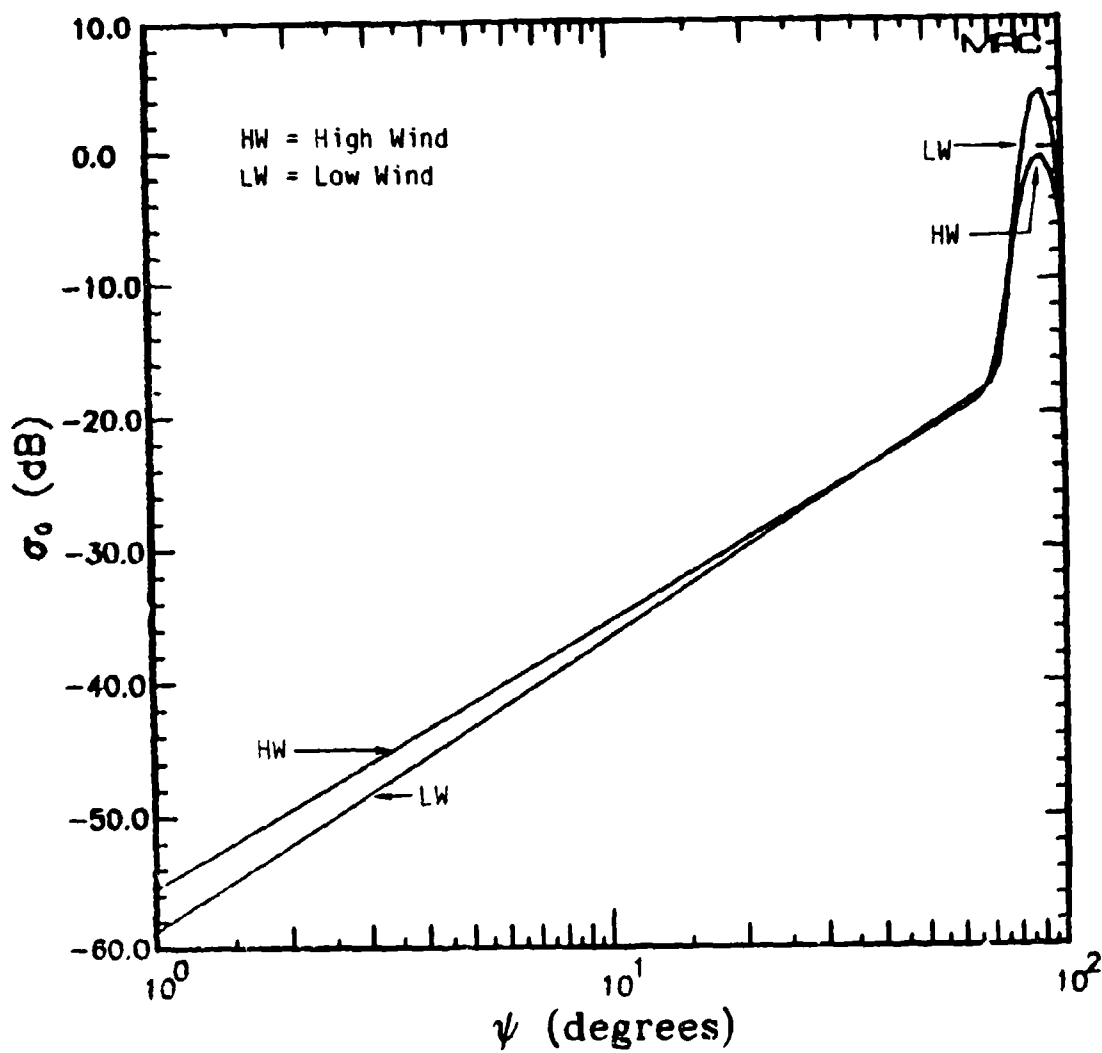
Figure 2. Modeled sea reflectivity vs. grazing angle and wind
conditions at L-band. (From Tomlinson Reference 6
and Long Reference 7.)

13

found them to provide a reasonable fit to reported data[3],[7] averaged over polarization and for grazing angles under about seventy degrees. The additional Gaussian terms have been added to provide a closer fit to data at high grazing angles.

SECTION 4

MAIN BEAM CLUTTER MODEL

Implementation of the method outlined above requires calculation of the mean power and doppler spectrum of the clutter signal. Temporarily neglecting the effect of range ambiguities, the illuminated area depicted in Figure 1 is defined in azimuth by the beamwidth and in elevation by the smaller of the elevation beamwidth or pulse length. These angular variations cause a doppler spread in the clutter signal through coupling to the SBR platform motion in the doppler equation

$$f = \frac{2v_s}{\lambda} \cos(EL) \cos(AZ) \tag{3}$$

$$\Delta f_{AZ} = \frac{2v_s}{\lambda} \cos(EL) \sin(AZ) \Delta AZ \tag{4}$$

$$\Delta f_{EL} = \frac{2v_s}{\lambda} \sin(EL) \cos(AZ) \Delta EL . \tag{5}$$

Equation 3 gives the mean doppler frequency as a function of the antenna geometry. Equations 4 and 5 give the 3dB spectral widths in azimuth and elevation, respectively. In the above equations

$$\Delta AZ = 3 \text{ dB two-way azimuth beamwidth } (AZ_3)$$
$$v_s = \text{satellite velocity}$$

and

$$\Delta EL = \text{minimum } (EL_3, c\tau_c \tan(\psi)/2R) \tag{6}$$

15

where

$$EL_3 = \text{3 dB two-way elevation beamwidth}$$

$$c = \text{speed of light}$$

$$\tau_c = \text{compressed pulse length}$$

$$R = \text{slant range}$$

Because of the high satellite velocities, the coupling between beamwidth and platform motion is usually the most important effect in determining doppler bandwidth. Since the antenna gain may be approximated by a Gaussian dependence, the azimuth and elevation doppler spreads are also Gaussian and their variances may be summed to yield a net spectral spread due to beamwidth effects

$$\sigma_B^2 = \sigma_{AZ}^2 + \sigma_{EL}^2 \tag{7}$$

where the standard deviations are related to the 3 dB spectral widths by

$$\sigma_{AZ} = .42 \; \Delta f_{AZ} \tag{8}$$

$$\sigma_{EL} = .42 \; \Delta f_{EL} \quad . \tag{9}$$

Internal or wave motion of the sea also broadens the doppler spectrum. Many measurements of sea clutter have yielded a Gaussian spectrum whose spread is related to the internal velocity spectral width of sea clutter, σ_v, as

$$\sigma_I = \frac{2\sigma_v}{\lambda} \quad . \tag{10}$$

This author is not aware of a good data base to predict values of σ_v that are applicable to the large illuminated areas viewed by an SBR. Existing measurements of the mean doppler shift and spectral spread utilize the smaller resolution cells of airborne and ground based radars.

16

Figures 3 and 4 show data for the spread, σ_v, and mean shifts respectively as a function of sea state. Typical high wind values for the spread and mean velocities are seen to be about 1 m/sec and 3 m/sec, respectively. Roughly speaking, for an SBR the mean shifts will be converted to a spectrum spread through the integration of a large number of smaller sized cells. Thus we can estimate an internal velocity spread of 3 or 4 m/sec for sea clutter viewed by an SBR. These numbers are consistent with the value of 5 m/sec suggested by Tomlinson[6]. The accuracy of this estimate will be improved as SBR measurement data becomes available.

Combining the effects of platform motion and internal motion yields a net doppler variance given by

$$\sigma_f^2 = \sigma_B^2 + \sigma_I^2 \quad . \tag{11}$$

We now consider the effects of ambiguous range returns. Figure 5a depicts the illuminated areas associated with the ambiguous range returns for a particular range bin. Doppler spectra are associated with the signal power returned from each one of these ambiguous clutter returns as discussed above. The signal voltage for this range bin is the sum of the signal voltages from the ambiguous returns. In the following we will refer to this simply as the sum voltage and to its doppler spectrum as the sum spectrum. Rather than generate statistical signal samples representing each ambiguous return and perform this sum directly, here we analytically compute the sum spectrum so that only the sum voltage requires statistical sampling on a pulse-to-pulse basis.

Returning again to the individual spectra of the ambiguous returns, we note that because of the dependence of elevation angle on range and also the dependence of doppler frequency on elevation angle, the mean doppler or center frequency of these spectra will vary over the

17
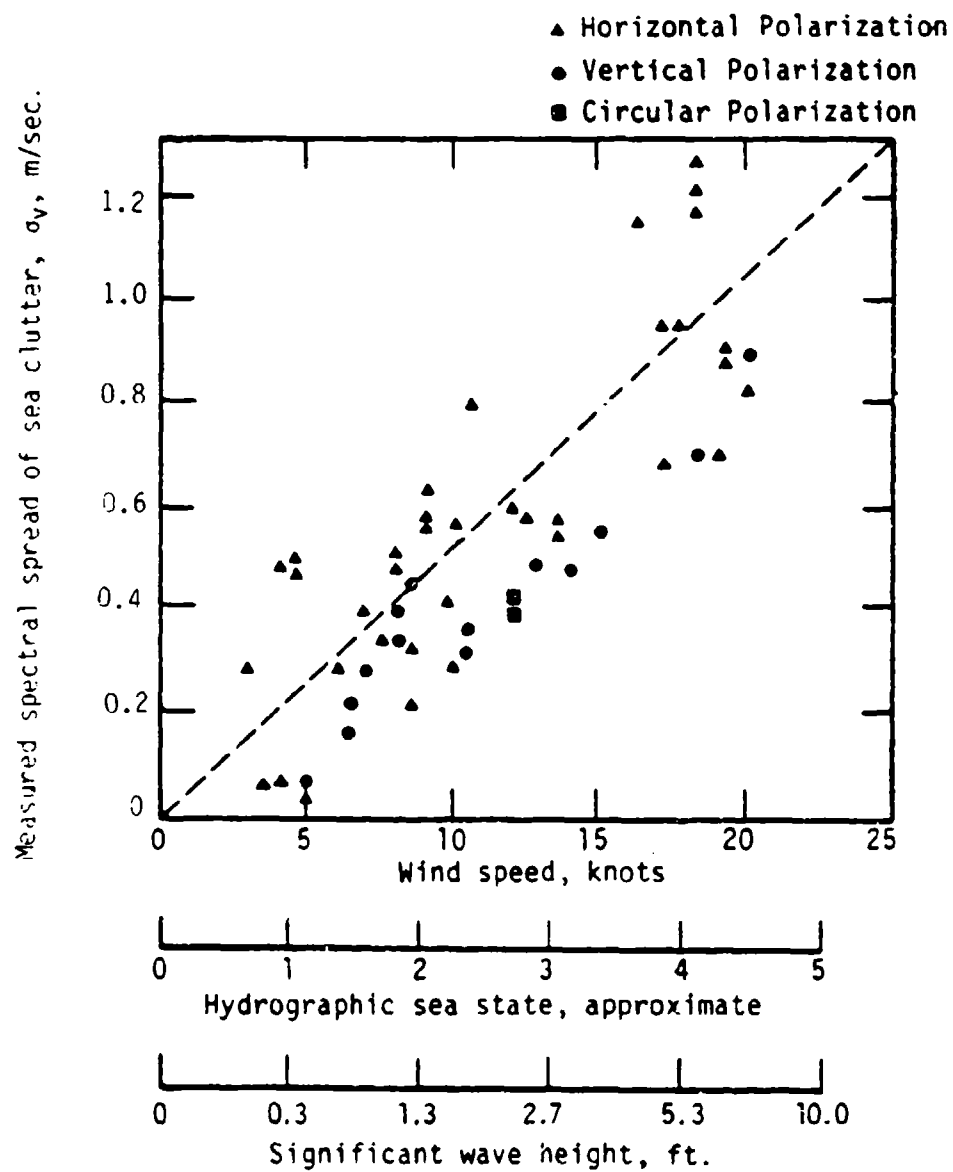
Figure 3. Variation of spectral spread for coherently detected sea clutter signals. (Data from Hicks et al., Kovaly et al., Currey, and Pidgeon, References 8-12).
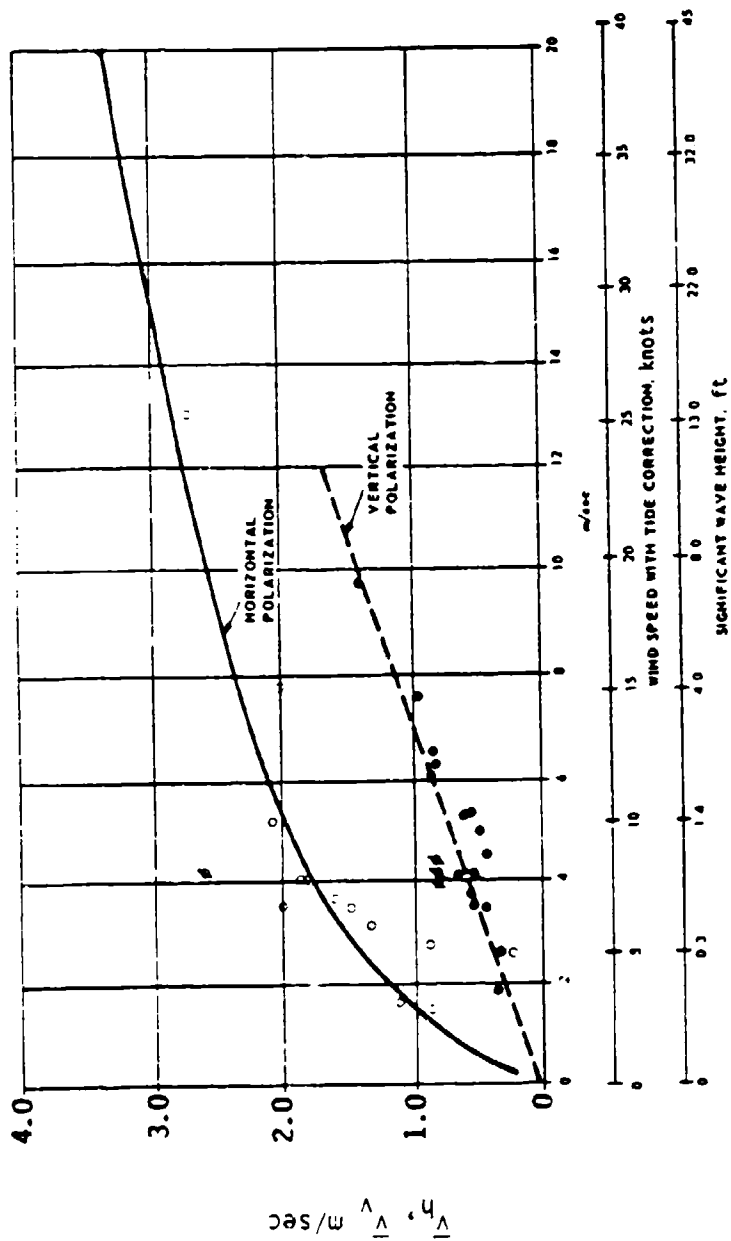
o *Horizontal polarization*; ● *vertical polarization*; ⓟ *bistatic data.*

Figure 4. Mean doppler shift for sea clutter signals (from Pidgeon's data, Reference 12).

19
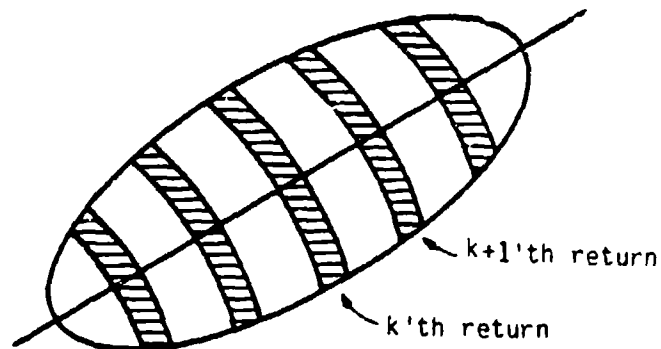
Figure 5a. Main beam footprint showing the illuminated areas of ambiguous range returns.
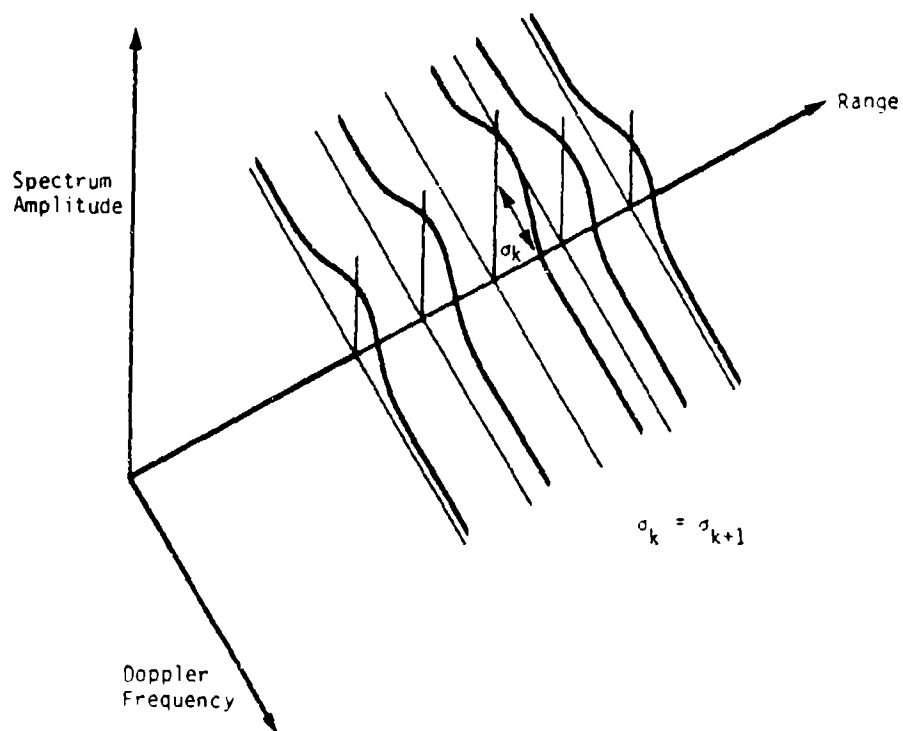
Figures 5b. Doppler spectra of the ambiguous returns with quadradic phase shift processing.

ambiguous returns. There exists a signal processing technique, QPSP, that can eliminate this doppler shift between ambiguous range returns. An explanation of how QPSP can be implemented will be given at the end of this section. For now we assume that QPSP can mitigate the doppler shifts between ambiguous returns as stated, and continue to investigate the properties of the sum signal.

Without QPSP the doppler spectral width of the sum signal due to ambiguous returns is determined by the antenna elevation beamwidth, since the center frequencies of the ambiguous returns vary with elevation angle. Since the individual spectra are independent, the net power is the sum of the individual powers of all the ambiguous returns.

With optimum implementation of QPSP, the spectra of the ambiguous returns have identical center frequencies as shown in Figure 5b. For this case the net power is still the sum of the individual powers, but the doppler spread of the sum signal is the same as that computed for one ambiguous return. This may be seen in the following.

The autocorrelation of the voltage from the k'th ambiguous return may be expressed as

$$R_k(\tau) = P_k R(\tau) \tag{12}$$

$$= \langle x_k(t)\, x_k^*(t+\tau)\rangle \tag{13}$$

where

$$P_k = \text{mean power of the k'th return}$$
$$x_k = \text{voltage of the k'th return} \quad .$$

This formulation is an explicit statement that the shape of the individual spectra are identical and hence the shape of the autocorrelation functions

21

are also identical since the antenna azimuth beamwidth is approximately constant over the antenna main lobe. The P_k's are not all equal since they depend on the antenna elevation gain which varies with ambiguous range. The autocorrelation of the sum signal from the combined ambiguous returns is then

$$R_\Sigma(\tau) = \langle (\sum_k x_k(t))(\sum_{k'} x_{k'}^*(t+\tau)) \rangle \qquad (14)$$

$$= \langle \sum_k x_k(t) \, x_k^*(t+\tau) \rangle \qquad (15)$$

since the ambiguous returns are independent. Making use of Equations 12 and 13, the autocorrelation of the sum voltage with QPSP may be expressed as

$$R_\Sigma(\tau) = R(\tau) \sum_k P_k \quad . \qquad (16)$$

Since the shape of the autocorrelation function given by Equation 16 is the same as that of the individual autocorrelation function, the shape of the sum spectrum will be the same as that of the individual spectrum. Therefore our modeling assumption is verified.

We now list the algorithms and equations needed to implement the above formulation.

4.1   MAIN BEAM CLUTTER POWER IN THE M'TH RANGE BIN

In this subsection an expression is given for the clutter contribution to the power received in the m'th range bin from all clutter sources within the footprint of the main beam. Several prerequisite calculations are first performed.

The range to the center of the main beam footprint is given by

$$R_c = -(r_0+h) \sin(EL_0) - \sqrt{(r_0+h)^2 \sin^2(EL_0) - (2r_0h+h^2)} \quad (17)$$

where

r_0 = earth's radius

h = satellite altitude

EL_0 = elevation angle of the LOS .

The grazing angle at the footprint center is

$$\Psi = \sin^{-1} \left\{ \frac{h}{R_c} (1+h/2r_0) - \frac{R_c}{2r_0} \right\} \quad (18)$$

and the change in range over the elevation beamwidth is

$$\Delta R_{EL} = 2R_c \left\{ \sin(2\Psi) \sin(EL_3/2) \right\} / \left\{ \cos(EL_3) - \cos(2\Psi) \right\} \quad (19)$$

The minimum and maximum ranges to the footprint are

$$R_{min} = R_c - \Delta R_{EL}/2 \quad (20)$$

$$R_{max} = R_c + \Delta R_{EL}/2 \quad (21)$$

The unambiguous range interval is

$$R_a = c/(2 \cdot PRF) \quad (22)$$

where PRF is the pulse repetition frequency. The number of range bins in an unambiguous range interval is then

$$M = R_a/\Delta r \quad (23)$$

23

where Δr is the range bin size and is determined by the radar video sampling rate. The range bin index for range R_{min} is

$$m_{min} = INT \{(MOD[R_{min}, R_a])M/R_a\} \qquad (24)$$

where $MOD(x,y)$ is equal to the remainder of the division x/y, and $INT(x)$ is equal to the largest integer whose magnitude does not exceed x.

The minimum range contributing to the m'th range bin

$$R_{m0} = R_{min} + (m-m_{min})\Delta r \quad ; \quad m \geq m_{min} \qquad (25)$$

$$R_{m0} = R_{min} + (M+m-m_{min})\Delta r; \quad m < m_{min} \qquad (26)$$

We can now determine if the range bin of interest (i.e., the bin with bin index m) is illuminated by the main beam. If R_{m0} is greater than R_{max}, the main beam does not return any clutter in bin number m. If R_{m0} is less than or equal to R_{max} there will be one or more ambiguous returns in bin m. If the number of ambiguous range returns is small, this method does not transition smoothly with respect to bins just inside and outside the beam footprint. If desired, the transition may be made more accurate by considering the fraction of the transmitted pulse which overlaps the footprint.

The number of contributing ambiguous range returns is

$$K = INT(\Delta R_{FL}/R_a) \quad . \qquad (27)$$

The range, grazing angle, and elevation angle to the k'th ambiguous area that contributes to the m'th range bin are given by

$$R_{mk} = R_{m0} + kR_a \qquad (28)$$

24

$$\psi_{mk} = \sin^{-1}\left\{\frac{h}{R_{mk}}\left(1 + \frac{h}{2r_0}\right) - \frac{R_{mk}}{2r_0}\right\} \tag{29}$$

$$EL_{mk} = -\sin^{-1}\left\{\frac{2r_0 h + h^2 + R_{mk}^2}{2 R_{mk}(r_0 + h)}\right\} \tag{30}$$

The illuminated area for the k'th ambiguous range and m'th range bin is given by

$$A_{mk} = \frac{\pi R_{mk}^2}{4} \quad EL_3 AZ_3 \csc(\psi_{mk}) \; ; \quad \tan(\psi_{mk}) > \frac{EL_3 R_{mk}}{c\,\tau_c/2} \tag{31}$$

$$A_{mk} = R_{mk} \quad AZ_3 \frac{c\,\tau_c}{2} \quad \sec(\psi_{mk}) \quad ; \quad \tan(\psi_{mk}) \leq \frac{EL_3 R_{mk}}{c\,\tau_c/2} \tag{32}$$

where τ_c = time duration of the received compressed pulse.

The mean RCS for this area is

$$RCS_{mk} = \sigma_0(\psi_{mk}) \cdot A_{mk} \tag{33}$$

where σ_0 is evaluated using Equation 1 or 2. The mean power for the m'th range bin is then given by the sum of the power from the contributing areas

$$P_m = \frac{P_t \lambda^2 \tau_t}{(4\pi)^3 \tau_c} \sum_{k=0}^{K-1} G(0, EL_{mk} - EL_0) \; RCS_{mk}/R_{mk}^4 \; . \tag{34}$$

where P_t = transmitted power

G = antenna 2-way power gain.

τ_t = time duration of the transmitted pulse.

25

We wish to remark at this time that the above algorithms are valid in a statistical sense only. While we have decided deterministically whether a particular range bin is illuminated by the main beam, we have neglected to account for certain effects such as atmospheric refraction which would cause an offset in range bin position relative to the main beam footprint. In support of this approach, we note that one range bin has no greater importance than any other as far as radar tracking performance is concerned; we are concerned only with the statistical effect on any one bin.

4.2 MAIN BEAM DOPPLER CENTER FREQUENCY
(neglecting the earth's rotation)

Without implementation of QPSP, the mean doppler frequency of the main beam clutter spectrum for the m'th range bin is given by

$$f_m = \frac{2v_s}{\lambda} \cos(EL_m) \cos(AZ_0) \tag{35}$$

where

$$EL_m = \frac{1}{K} \sum_{k=0}^{K-1} EL_{mk} \tag{36}$$

is the average elevation angle of the ambiguous returns for the m'th range bin. Equation 36 gives the elevation angle as the average over the returns from the K ambiguous ground areas that arrive simultaneously to contribute to the m'th range bin.

With QPSP the mean frequency of the ambiguous returns depends upon the pulse to which the inverse phase processing is matched. For modeling purposes the exact value is not important and as a convention we let

$$f_m = \frac{2v_s}{\lambda} \cos(EL_{m0}) \cos(AZ_0) \quad . \tag{37}$$

26

4.3   MAIN BEAM DOPPLER SPREAD
   (neglecting the earth's rotation)

The doppler standard deviation due to internal motion is given by Equation 10 with σ_v nominally 4 m/sec.

Doppler standard deviations due to platform motion are given by

$$\sigma_{AZ} = \frac{.84 \ v_s}{\lambda} \cos\left(EL_o\right) \sin\left(AZ_o\right) AZ_3 \tag{38}$$

$$\sigma_{EL} = \frac{.84 \ v_s}{\lambda} \sin\left(EL_o\right) \cos\left(AZ_o\right) \Delta EL \tag{39}$$

where

$$\Delta EL = \text{Maximum} \left(\left|EL_{mK}-EL_{ml}\right|, \ c\tau_c \tan(\psi)/2R_c\right) \tag{40}$$

without QPSP, and

$$\Delta EL = \text{Minimum} \left(EL_3, \ c\tau_c \tan(\psi)/2R_c\right) \tag{41}$$

with QPSP.

The net variance of the spectrum is obtained by summing the variances due to platform motion and to internal motion (Equations 7 and 11).

4.4   DOPPLER EFFECTS INCLUDING THE EARTH'S ROTATION

Referring to Figures 6a and 6b, it is assumed that the SBR location is given in geocentric coordinates by

27
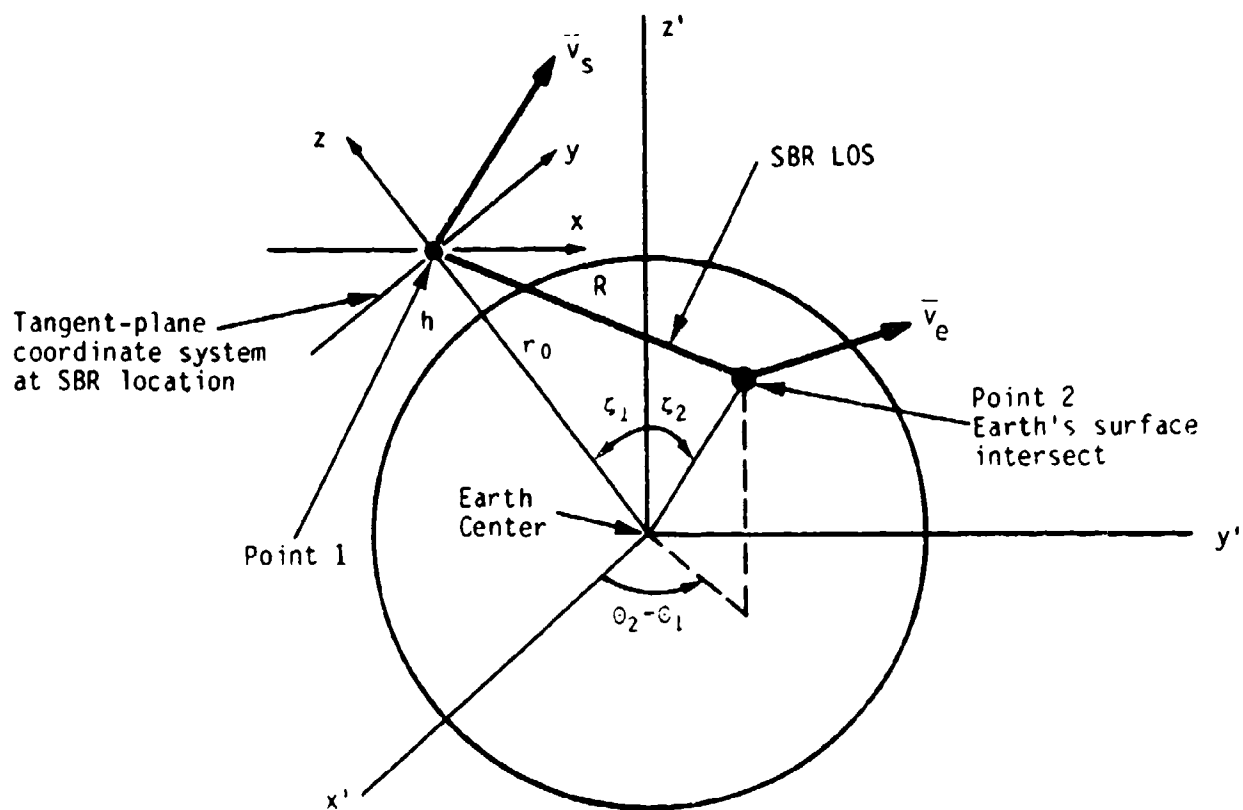
Figure 6a. SBR and earth rotational velocities for doppler calculation.
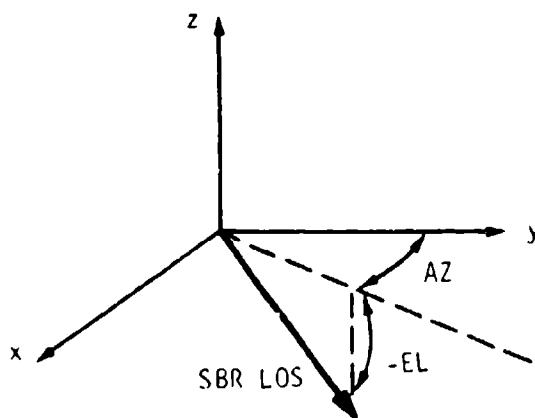
Figure 6b. SBR LOS in the tangent-plane coordinate system.

28

$$\theta_1 = \text{SBR longitude} \qquad\qquad (-\pi < \theta_1 < \pi)$$

$$\zeta_1 = \text{SBR colatitude}$$

$$h = \text{SBR altitude}$$

and that the azimuth, elevation angles of the SBR LOS are given in the x, y, z tangent plane coordinate system by

$$AZ = \text{LOS azimuth}$$

$$EL = \text{LOS elevation (negative when looking down)} .$$

The tangent-plane coordinate system is a cartesian coordinate system with x directed to the east, y to the north, and z vertically.

We must first find the geocentric coordinates (θ_2, ζ_2) of the LOS intersection with the earth's surface.

The location of the intersection in the x', y', z' cartesian coordinate system is given by

$$x_2' = \{R \sin(\zeta_1) \sin(EL) - R \tan(\theta_1) \cos(EL) \sin(AZ)$$

$$- R \cos(\zeta_1) \cos(EL) \cos(AZ) + (h+r_0) \sin(\zeta_1)\}$$

$$/\{\cos(\theta_1) + \sin(\theta_1) \tan(\theta_1)\} \tag{42}$$

$$y_2' = R \cos(EL) \sin(AZ)/\cos(\theta_1) + \tan(\theta_1) x_2' \tag{43}$$

for $|\theta_1| \leq \pi/4$ or $|\theta_1| \geq 3\pi/4$ (case a) and by

$$y_2' = \{R \sin(\zeta_1) \sin(EL) + R \cot(\theta_1) \cos(EL) \sin(AZ)$$

$$- R \cos(\zeta_1) \cos(EL) \cos(AZ) + (h+r_0) \sin(\zeta_1)\}$$

$$/\{\sin(\theta_1) + \cos(\theta_1) \cot(\theta_1)\} \tag{44}$$

$$x_2' = - R \cos(EL) \sin(AZ)/\sin(\theta_1) + \cot(\theta_1) y_2' \tag{45}$$

29

for $\pi/4 < |\theta_1| < 3\pi/4$ (case b) where R is the slant range found through Equation 17 and

$$z_2' = \{r_0{}^2 - (x_2')^2 - (y_2')^2\}^{1/2} \ . \tag{46}$$

The geocentric coordinates of the intersection point (θ_2, ς_2) are then

$$\theta_2 = \tan^{-1}(y_2'/x_2') \tag{47}$$

$$\varsigma_2 = \cos^{-1}(z_2'/r_0) \ . \tag{48}$$

4.5 MAIN BEAM DOPPLER CENTER FREQUENCY

The doppler frequency of a point on the earth's surface is

$$f_m = \frac{2}{\lambda} \ (\overline{v}_s - \overline{v}_e) \cdot \hat{R} \tag{49}$$

where

$\overline{v}_s$ = satellite velocity vector

$\overline{v}_e$ = earth's surface rotational velocity

$\hat{R}$ = unit vector along the LOS.

The satellite velocity vector in the x, y, z coordinate system is assumed to be known and is given by

$$\overline{v}_s = v_{sx}\hat{x} + v_{sy}\hat{y} + v_{sz}\hat{z} \ . \tag{50}$$

$\hat{R}$ is found to be

$$\hat{R} = \sin(AZ)\cos(EL)\hat{x} + \cos(AZ)\cos(EL)\hat{x} + \sin(EL)\hat{z} \ . \tag{51}$$

In the geocentric coordinate system

$$\overline{v}_e = \omega_e r_0 \sin(\zeta_2)\hat{\theta} \tag{52}$$

where ω_e is the earth's radian frequency of rotation.

By transforming $\overline{v}_e$ to the x, y, z coordinate system the dot product in Equation 49 may be evaluated to obtain

$$f_m = \frac{2}{\lambda} \{ (v_{sx} - \omega_e r_0 \sin(\zeta_2) \cos(\theta_2 - \theta_1)) \sin(AZ) \cos(EL)$$

$$+ (v_{sy} - \omega_e r_0 \sin(\zeta_2) \cos(\zeta_1) \sin(\theta_2 - \theta_1)) \cos(AZ) \cos(EL)$$

$$+ (v_{sz} + \omega_e r_0 \sin(\zeta_2) \sin(\zeta_1) \sin(\theta_2 - \theta_1)) \sin(EL) \} \ . \tag{53}$$

4.6 MAIN BEAM DOPPER SPREAD

Doppler spread due to beamwidth effects may be found by taking the deriative of Equation 49 with respect to AZ and EL.

$$\sigma_{AZ} = .42 \ \left| \partial f_m / \partial AZ \right| \ AZ_3 \tag{54}$$

$$\sigma_{EL} = .42 \ \left| \partial f_m / \partial EL \right| \ \Delta EL \tag{55}$$

where ΔEL is given by Equation 40, without QPSP or by 41 if QPSP is implemented.

Referring to Equations 53 and 42 through 48, f_m depends implicitly on AZ, EL through θ_2, ζ_2 as well as explicitly. Expressing f_m in the form

$$f_m = \frac{2}{\lambda} \{ A \sin(AZ) \cos(EL) + B \cos(AZ) \cos(EL) + C \sin(EL) \} \tag{56}$$

31

where

$$A = v_{sx} - \omega_e r_0 \sin(\zeta_2) \cos(\theta_2 - \theta_1) \tag{57}$$

$$B = v_{sy} - \omega_e r_0 \sin(\zeta_2) \cos(\zeta_1) \sin(\theta_2 - \theta_1) \tag{58}$$

$$C = v_{sz} + \omega_e r_0 \sin(\zeta_2) \sin(\zeta_1) \sin(\theta_2 - \theta_1) \tag{59}$$

The doppler spread due to azimuth beamwidth is

$$
\begin{aligned}
\sigma_{AZ} = \frac{.84 \, AZ_3}{\lambda} \Big\{ & A \cos(AZ) \cos(EL) - B \sin(AZ) \cos(EL) + \sin(AZ) \cos(EL) \\
& \cdot \left[-\omega_e r_0 \cos(\zeta_2) \cos(\theta_2 - \theta_1) \frac{\partial \zeta_2}{\partial AZ} + \omega_e r_0 \sin(\zeta_2) \sin(\theta_2 - \theta_1) \frac{\partial \theta_2}{\partial AZ} \right] \\
& - \cos(AZ) \cos(EL) \cdot \left[\omega_e r_0 \cos(\zeta_2) \cos(\zeta_1) \sin(\theta_2 - \theta_1) \frac{\partial \zeta_2}{\partial AZ} \right. \\
& \left. + \omega_e r_0 \sin(\zeta_2) \cos(\zeta_1) \cos(\theta_2 - \theta_1) \frac{\partial \theta_2}{\partial AZ} \right] + \sin(EL) \\
& \cdot \left[\omega_e r_0 \cos(\zeta_2) \sin(\zeta_1) \sin(\theta_2 - \theta_1) \frac{\partial \zeta_2}{\partial AZ} \right. \\
& \left. + \omega_e r_0 \sin(\zeta_2) \sin(\zeta_1) \cos(\theta_2 - \theta_1) \frac{\partial \theta_2}{\partial AZ} \right] \Big\} \; .
\end{aligned}
\tag{60}
$$

The doppler spread due to elevation beamwidth is

$$
\begin{aligned}
\sigma_{EL} = \frac{.84 \, \Delta EL}{\lambda} \Big\{ & -A \sin(AZ) \sin(EL) - B \cos(AZ) \sin(EL) + C \cos(EL) \\
& + \sin(AZ) \cos(EL) \cdot \left[-\omega_e r_0 \cos(\zeta_2) \cos(\theta_2 - \theta_1) \frac{\partial \zeta_2}{\partial EL} \right. \\
& \left. + \omega_e r_0 \sin(\zeta_2) \sin(\theta_2 - \theta_1) \frac{\partial \theta_2}{\partial EL} \right] - \cos(AZ) \cos(EL)
\end{aligned}
$$

$$\cdot \left[\omega_e r_0 \cos(\zeta_2) \cos(\zeta_1) \sin(\theta_2 - \theta_1) \frac{\partial \zeta_2}{\partial EL} \right.$$

$$\left. + \omega_e r_0 \sin(\zeta_2) \cos(\zeta_1) \cos(\theta_2 - \theta_1) \frac{\partial \theta_2}{\partial EL} \right] + \sin(EL)$$

$$\cdot \left[\omega_e r_0 \cos(\zeta_2) \sin(\zeta_1) \sin(\theta_2 - \theta_1) \frac{\partial \zeta_2}{\partial EL} \right.$$

$$\left. \left. + \omega_e r_0 \sin(\zeta_2) \sin(\zeta_1) \cos(\theta_2 - \theta_1) \frac{\partial \theta_2}{\partial EL} \right] \right\} \quad . \tag{61}$$

The partial derivatives of θ_2, ζ_2 may be found from Equations 47 and 48

$$\frac{\partial \theta_2}{\partial AZ} = \frac{1}{1 + (y_2'/x_2')^2} \left\{ \frac{\frac{\partial y_2'}{\partial AZ}}{x_2'} - \frac{y_2' \frac{\partial x_2'}{\partial AZ}}{(x_2')^2} \right\} \tag{62}$$

and similarly for $\dfrac{\partial \theta_2}{\partial EL}$

$$\frac{\partial \zeta_2}{\partial AZ} = \frac{x_2' \frac{\partial x_2'}{\partial AZ} + y_2' \frac{\partial x_2'}{\partial AZ}}{r_0 z_2' \sqrt{1 - (z_2'/r_0)^2}} \tag{63}$$

and similarly for $\dfrac{\partial \zeta_2}{\partial EL}$.

The remaining chore is to solve for the partial derivatives of x_2', y_2' using Equations 42 through 46. First we obtain the derivatives with respect to azimuth. For case a we have

$$\frac{\partial x_2'}{\partial AZ} = \{-R \tan(\theta_1) \cos(EL) \cos(AZ) + R \cos(\zeta_1) \cos(EL) \sin(AZ)\}$$

$$/\{\cos(\theta_1) + \sin(\theta_1) \tan(\theta_1)\} \tag{64}$$

33

$$\frac{\partial y_2'}{\partial AZ} = R \cos(EL) \cos(AZ)/\cos(\theta_1) + \tan\theta_1 \frac{\partial x_2'}{\partial AZ} \qquad (65)$$

and for case b

$$\frac{\partial y_2'}{\partial AZ} = \{R \cot(\theta_1) \cos(EL) \cos(AZ) + R \cos(\varsigma_1) \cos(EL) \sin(AZ)\}$$

$$/\{\sin(\theta_1) + \cos(\theta_1) \cot(\theta_1)\} \qquad (66)$$

$$\frac{\partial x_2'}{\partial AZ} = -R \cos(EL) \cos(AZ)/\sin(\theta_1) + \cot(\theta_1) \frac{\partial y_2'}{\partial AZ} \quad . \qquad (67)$$

For the derivative with respect to elevation we first need

$$\frac{\partial R}{\partial EL} = -(r_0+h) \cos(EL) - (r_0+h)^2 \sin(EL) \cos(EL)$$

$$/\sqrt{(r_0+h)^2 \sin^2(EL) - (2r_0h+h^2)} \quad . \qquad (68)$$

The elevation derivatives are then given for case a by

$$\frac{\partial x_2'}{\partial EL} = \{\cos(\theta_1) + \sin(\theta_1) \tan(\theta_1)\}^{-1}$$

$$\cdot \left\{ \frac{\partial R}{\partial EL} [\sin(\varsigma_1) \sin(EL) - \tan(\theta_1) \cos(EL) \sin(AZ) \right.$$

$$- \cos(\varsigma_1) \cos(EL) \cos(AZ)] + R [\sin(\varsigma_1) \cos(EL)$$

$$\left. + \tan(\theta_1) \sin(EL) \sin(AZ) + \cos(\varsigma_1) \sin(EL) \cos(AZ)] \right\}$$

$$\qquad (69)$$

$$\frac{\partial y_2'}{\partial EL} = \sec(\theta_1) \cdot \{\partial R/\partial EL \cos(EL) \sin(AZ) - R \sin(EL) \sin(AZ)\}$$

$$\qquad (70)$$

and for case b by

$$\frac{\partial y_2'}{\partial EL} = \{\sin(\theta_1) + \cos(\theta_1)\cot(\theta_1)\}^{-1}$$

$$\cdot \left\{ \frac{\partial R}{\partial EL} \left[\sin(\varsigma_1)\sin(EL) + \cot(\theta_1)\cos(EL)\sin(AZ) \right. \right.$$

$$- \cos(\varsigma_1)\cos(EL)\cos(AZ) \right] + R\left[\sin(\varsigma_1)\cos(EL) \right.$$

$$\left. \left. - \cot(\theta_1)\sin(EL)\sin(AZ) + \cos(\varsigma_1)\sin(EL)\cos(AZ) \right] \right\} \quad .$$

$$(71)$$

$$\frac{\partial x_2'}{\partial EL} = \csc(\theta_1) \cdot \left\{ -\frac{\partial R}{\partial EL}\cos(EL)\sin(AZ) + R\sin(EL)\sin(AZ) \right\} \quad .$$

$$(72)$$

In summary, these algorithms may be used to find the doppler spreads by first calculating $\partial R/\partial EL$ and then the partial derivatives of x_2' and y_2' with respect to AZ and EL. With these quantities the partial derivatives of θ_2, ς_2 with respect to AZ, EL may be computed and then used to solve for the doppler spread through Equations 54 and 55.

Practically speaking, it is probably computationally less burdensome to solve for the doppler spreads by differencing Equation 53 over the beamwidths, although this approach does require solving for the four earth intersection points which define the mainbeam footprint. Before choosing either method, the accuracy and computational efficiency of each should be compared. For low altitude orbits the simpler equations derived without inclusion of the earth's rotational effects are approximately correct and may be utilized.

35

4.7   QUADRATIC PHASE SHIFT PROCESSING (QPSP)

The purpose of QPSP is to reduce the doppler spread of the main beam clutter spectrum by compensating for the shift in doppler center frequencies of the ambiguous range returns. Modeling the doppler spread with or without QPSP was discussed earlier in this section. We now describe the basis for the signal processing involved in QPSP.

In this technique the phase is shifted quadratically in one direction as a function of pulse number on transmit, and in the opposite direction on receive. We assume that a phase shift modulation

$$\phi_t = \epsilon p^2 \tag{73}$$

is implemented on a pulse-to-pulse basis within a sequence of transmitted pulses where p is pulse number. On receive, the range-gated signal may contain main beam clutter power returned from one or more of the transmitted pulses. When there is more than one contributing pulse, these multiple and simultaneously received pulses are called ambiguous range returns. We use the index k once again to designate the ambiguous range number, with k increasing with increasing range, and choose a time reference such that the sampling time when the p'th pulse is the zeroth ambiguous return is pT. As an example, in Figure 7 we show the relation of pulse number to ambiguous range index and sampling time for the case that there are five contributing ambiguous returns. Then the phase on the k'th ambiguous return at time pT is given by

$$\phi_{tk}(pT,k) = \epsilon(p-k)^2 \ . \tag{74}$$

We assume that a quadratic phase shift of the opposite sign is applied on receive

$$\phi_r(pT,k) = -\epsilon(p-\Delta p)^2 \tag{75}$$

36
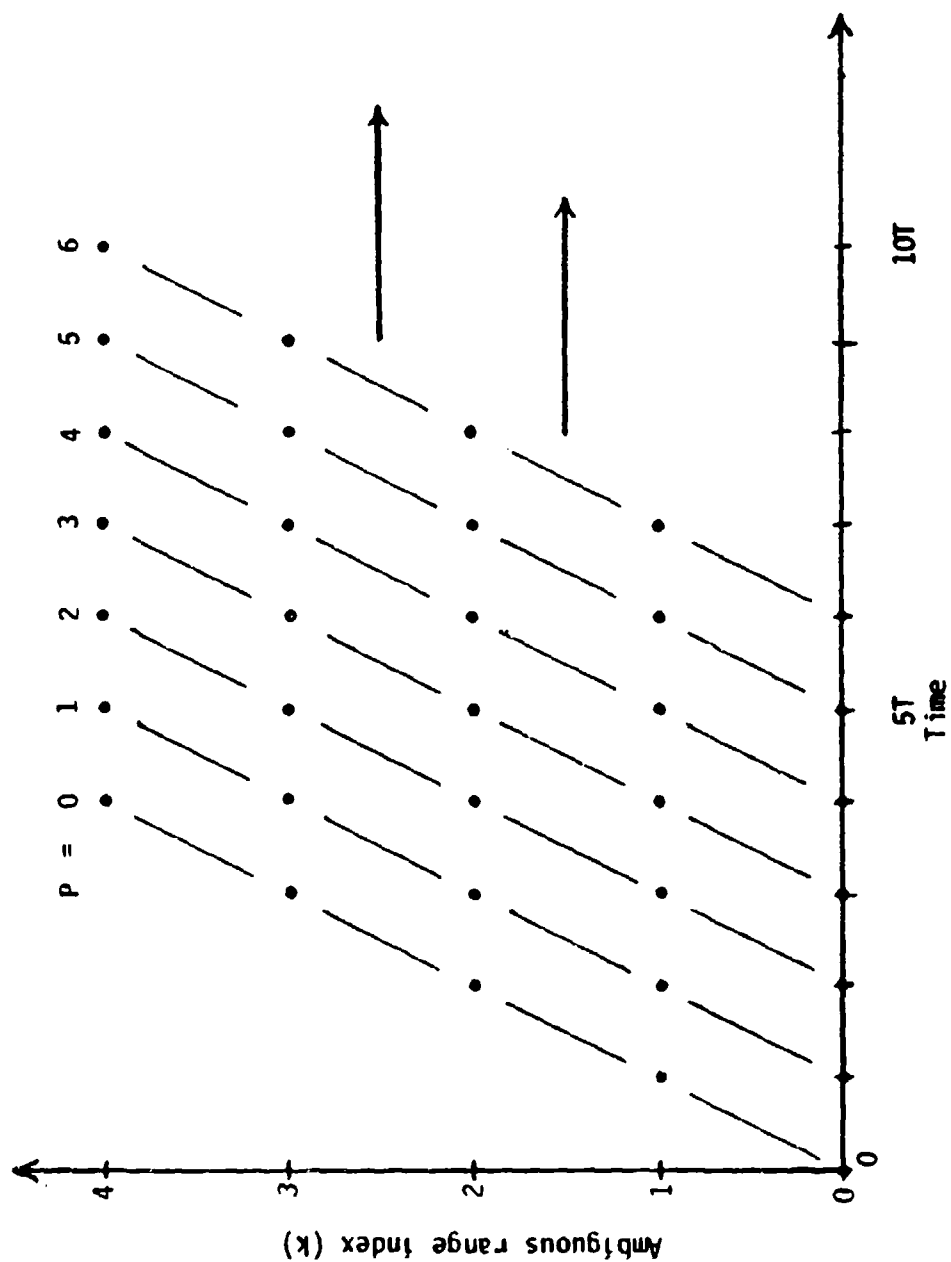
Figure 7. Pulse number versus sampling time and ambiguous range index.

where the offset Δp reflects the fact that the inverse phase shift processing in general may not be matched to that of the transmitted phase modulation.

The net phase modulation on the k'th ambiguous return at time pT is then

$$\phi_{net}(pT,k) = \epsilon(k^2 - \Delta p + 2p\Delta p - 2pk) \qquad (76)$$

and the doppler shift of the k'th ambiguous return is then

$$\Delta f(k) = \frac{1}{2\pi} \frac{d\phi_{net}(pT,k)}{dpT} = \epsilon\Delta p/\pi T - \epsilon k/\pi T \quad . \qquad (77)$$

QPSP is seen to impose a frequency shift that varies linearly with ambiguous range index.

The doppler shift of the k'th ambiguous return due to the elevation angle difference is given by

$$\Delta f_{EL}(k) = \frac{2v_s}{\lambda} \sin(EL_0) \cos(AZ_0) \Delta EL(k) \qquad (78)$$

where

$$\Delta EL(k) \approx R_a k \tan(\psi_0)/R_c \qquad (79)$$

For ease of interpretation we have used the expression for Δf_{EL} neglecting the earth's rotational effects. For the frequency shift from processing to cancel that due to ambiguous range we require

$$\Delta f_{EL}(k) = -\epsilon k/\pi T \qquad (80)$$

38

since the first term in Equation 77 is a frequency offset which is constant with respect to ambiguous range. Using Equations 78 and 79 to solve Equation 77 for ϵ we obtain

$$\epsilon = -2\pi v_s R_a T \sin(EL_0) \cos(AZ_0) \tan(\psi_0)/\lambda R_c \quad . \qquad (81)$$

If we had used the expression for Δf_{EL} that accounted for the earth's rotational effects in the above derivation, ϵ would still have been calculable in the same manner.

In summary, QPSP has been shown to be an effective technique for mitigating the doppler shift of ambiguous returns. This has the desirable result of increasing the clutter free doppler bandwidth available to a pulse doppler radar. When applied in an optimum sense it requires implementation as a function of look angle.

SECTION 5
SIDELOBE CLUTTER MODEL

This section is devoted to the calculation of the clutter power spectrum that is caused by returns from outside the main beam footprint. Because of an SBR's large field of view, the clutter signal received through the antenna sidelobes will contain multiple ambiguous range returns. The illuminated area for the sidelobe return in a given range bin is a series of annular rings corresponding to the pulse length limited areas of the ambiguous returns. Mean power of the sidelobe return may be taken to be the same for all range bins, since the ambiguous returns for different bins will sample essentially the same areal portion of the earth's surface.

To calculate the mean power we must sum the power contributions from the ambiguous returns. It is desirable to estimate the range at which the power returned becomes negligible so that the number of ambiguous returns to be summed may be reduced accordingly. The power per ambiguous return falls off at least as fast as the reflectivity function σ_0. By referring to Figure 3 we see that for both the HW and LW models σ_0 has decreased by more than 20 dB from its peak value at a grazing angle of 50 degrees. The range at which this occurs is given by

$$R_{50} = -r_0 \sin(50°) + \sqrt{r_0^2 \sin^2(50°) + (2r_0 h + h^2)} \qquad . \qquad (82)$$

Thus, we need only consider returns for ranges less than R_{50}. As an Example, for a low altitude (1400nm) orbit and a PRF less than 10 KHz, fewer than 17 ambiguous returns are important for calculation of the required power.

40

The doppler spectrum of the sidelobe clutter return is not amenable to simple analytic treatment. For the special case of low altitude orbits of primary concern here, the clutter spectral bandwidth will be shown to be wider than the PRF. In addition, the sidelobe clutter may be treated as being uncorrelated on a pulse-to-pulse basis.

The doppler spectral bandwidth is dominated by the coupling between platform motion and the antenna beamwidth. Since the sidelobe gain may be assumed to be omnidirectional, the beamwidth of interest is defined by the angular section of the earth's surface contributing to the sidelobe return as viewed by the SBR. Referring to Figure 8, the doppler shifts of a return from a grazing angle ψ are given by

$$\Delta f_s(\psi) = 2 \, v_s r_0 \cos(\psi) / \lambda(r_0 + h) \tag{83}$$

$$\Delta f_e(\psi) = 2 \, v_e \cos(\psi) / \lambda \tag{84}$$

where $\Delta f_s(\psi)$ and $\Delta f_e(\psi)$ are the shifts due to satellite and earth motion, respectively. The SBR orbit is assumed to be circular. These are the shifts when the satellite and earth's surface velocity vectors are coplanar with the LOS and the nadir point so that they are the maximum shifts for a given grazing angle.

Relying once again on consideration of the sea reflectivity as a function of grazing angle, it is seen that the principle contribution to the sidelobe return results from grazing angles of 80 degrees and larger. Using the doppler shifts for a grazing angle of 80 degrees to estimate the spectral width, the minimum spectral width occurs when the satellite and earth motion shifts subtract and is given by

$$\sigma_{min} = \left| \Delta f_s(80°) - \Delta f_e(80°) \right| \; . \tag{85}$$

Figure 9 shows the doppler shifts predicted by Equations 83 and 84 for a

41
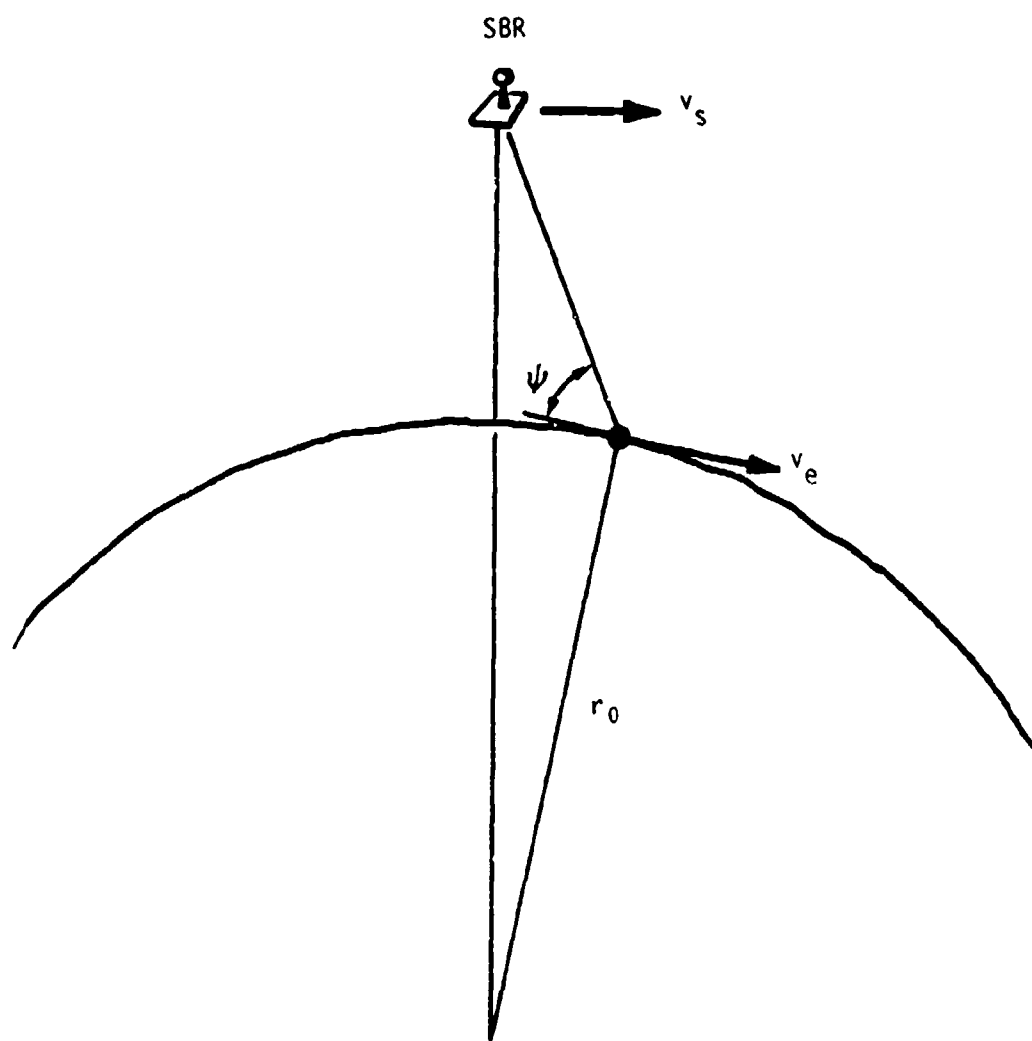
Figure 8.   Geometry for sidelobe doppler analysis.

42
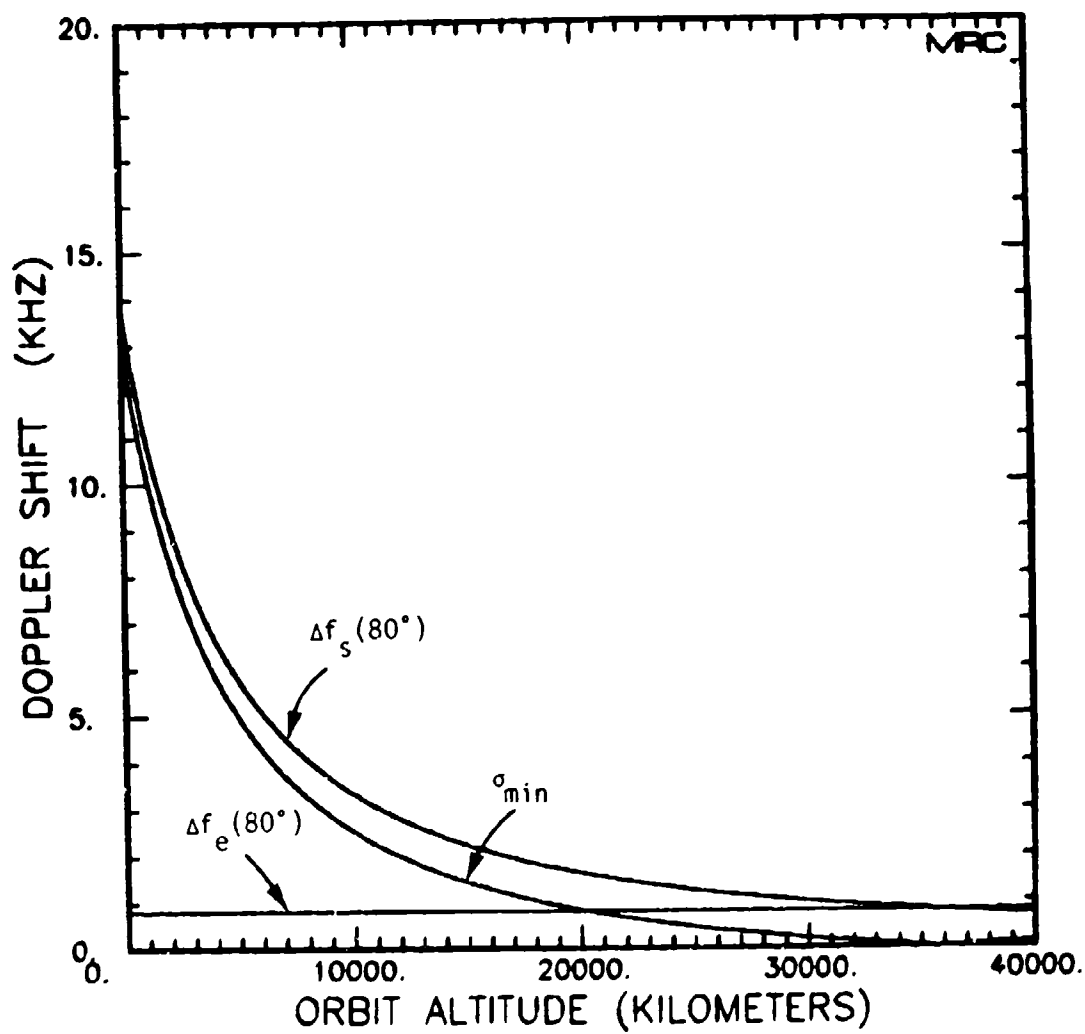
Figure 9. Sidelobe clutter doppler shifts.

43

grazing angle of 80 degrees as a function of orbit altitude. Also shown on the figure is the one sided spectral width σ_{min}. We note that the two sided spectral width is greater than 10 KHz for orbit altitudes less then ≈5,000 kilometers (≈2,700 nm). Since we are primarily interested in this range of orbits and for PRFs equal to about 10 KHz and smaller, the sidelobe return may be modeled as a flat spectrum, similar to additive white noise.

5.1 SIDELOBE CLUTTER POWER IN THE M'TH RANGE BIN

The number of ambiguous range returns considered is

$$K_{SL} = INT \left| (R_{50} - h)/R_a \right| \tag{86}$$

where R_{50} is obtained through Equation 82.

The range, grazing angle, and illuminated area of the k'th ambiguous return are given by

$$R_k = h + (k-1) \cdot R_a \tag{87}$$

$$\psi_k = \sin^{-1} \frac{h}{R_k} \left\{ (1 + \frac{h}{2r_0}) - \frac{R_k}{2r_0} \right\} \tag{88}$$

$$A_k = \Pi c \tau_c R_k \tag{89}$$

The mean power of the k'th return is

$$P_k = \frac{P_t \lambda^2 G_{SL} c \tau_t}{64 \Pi^2} \frac{\sigma_0(\psi_k)}{R_k^3} \tag{90}$$

where G_{SL} is the average two-way antenna sidelobe gain.

The mean power in any range bin is then given by

$$\sum_{K=0}^{K_{SL}-1} P_K \cdot \tag{91}$$

44

REFERENCES

1. Mitchell, R. L., Radar Signal Simulation, Artech House, Inc., 1976.

2. Paul et,al - Grumman, Owen et.al - Raytheon, "Space-Based Radar Surveillance System Study. Final Report for Phase II." Grumman Aerospace Corporation, January 1978, unpublished.

3. Nathanson, Fred E., Radar Design Principles, McGraw Hill, New York, 1969.

4. Skolnik, M. I., Radar Handbook, McGraw-Hill Book Company, New York, 1970.

5. Knepp, D. L., and R. A. Dana, "The Impact of Strong Scintillation on Space Based Radar Design - Clutter Rejection," MRC-R-787, Mission Research Corporation, October 1983.

6. Tomlinson, P. G., "A Model for Space Based Radar Clutter," Decision-Science Applications, Inc., RADC-TR-79-166, June 1979.

7. Long, Maurice W., Radar Reflectivity of Land and Sea, D. C. Heath and Company, Lexington, 1975.

8. Hicks, B. L., et.al., "Sea Clutter Spectrum Studies Using Airborne Coherent Radar," Univ. Illinois Control Sys. Lab., Rept. 37, June 26, 1953.

9. Kovaly, J. J., et.al., "Sea Clutter Studies Using Airborne Coherent Radar," Univ. Illinois Control Sys. Lab., Rept. 37, June 26, 1953.

10. Currey, G. R., "A Study of Radar Clutter in Tradex," M.I.T. Lincoln Lab. Group Report 164-29, May 25, 1964 (also IRE Trans., Vol. MIL9, no. 1, pp. 39-44, January 1965).

11. Pidgeon, V. W., "Time, Frequency, and Spacial Correlation of Radar Sea Return," Space Sys. Planetary Geol. Geophys., American Astronautical Society, May 1967.

12. Pidgeon, V. W., "The Doppler Dependence of Radar Sea Return," J. Geophys. Res., Februrary 15, 1968.

APPENDIX

A STATISTICAL SIGNAL GENERATION TECHNIQUE
FOR REALIZING THE SAMPLE CLUTTER VOLTAGE
(D. L. Knepp)

In this appendix, a numerical technique is described to generate realizations or sample functions of the video clutter voltage received by a pulse doppler SBR. The goal of this technique is to generate the two quadrature components of the clutter signal as received at a single range gate for all the pulses of a coherent pulse train or coherent dwell. It will be shown that this technique requires knowledge of the mean clutter spectrum and depends upon the observation that the clutter voltage has a Gaussian probability distribution with uncorrelated quadrature components. An identical statistical signal technique is used by Knepp[1] to generate realizations of the phase for a multiple phase screen propagation simulation.

Assume that there are N pulses per coherent pulse train separated in time by the quantity T so that the pulse repetition frequency (PRF) is 1/T. As will be shown, the clutter voltage c(nT), is generated from initial knowledge of its mean power spectrum. In continuous notation, the clutter voltage may be written as the Fourier transform

$$c(t) = \int_{-\infty}^{\infty} C(\omega) e^{i\omega t} d\omega \qquad (A-1)$$

1. "Multiple Phase-Screen Calculation of the Temporal Behavior of Stochastic Waves," Proc. IEEE, Vol. 71, No. 6, pp. 722-737, June 1983.

In the discrete* case, Equation A-1 is written as

$$c(nT) = \sum_{m=0}^{N-1} \hat{C}(m\Delta\omega)e^{i2\pi mn/N} \Delta\omega \quad n=0,\ldots,N-1 \tag{A-2}$$

Now if the Fourier transform of the clutter spectrum was available, a clutter voltage realization could be easily generated by using Equation A-2. For the moment let us choose as the Fourier transform the quantity

$$\hat{C}(m\Delta\omega) = r_m[C(m\Delta\omega)NT/2\pi]^{1/2} \tag{A-3}$$

where $C(m\Delta\omega)$ represents discrete values of the known desired mean clutter power spectrum. In the following it is proven that this choice is correct. Here $\Delta\omega = 2\pi/NT$, NT is the time duration of the dwell, and therefore $T\Delta\omega = 2\pi/N$. r_m is a complex number given as the sum of two independent Gaussian random variables with zero mean and variances of unity.

$$r_m = \sqrt{1/2} \, (g_{1m} + ig_{2m}) \tag{A-4}$$

Successive values of g_{1m} and g_{2m} may be obtained numerically by sampling from a pseudo-random sequence of numbers with a Gaussian distribution. The factor of $\sqrt{1/2}$ is included so that

$$\langle r_m r_n^{\star} \rangle = \delta_{mn} \tag{A-5}$$

where δ_{mn} is the Kroneker delta function. It is apparent that with the above choice for r_m, $c(nT)$ is the sum of a sequence of Gaussian variates

---

* In this appendix all discrete sums are taken over a range of the index from 0 to N-1.

and thus its real and imaginary parts (i.e., its quadrature components) both have a Gaussian or normal probability distribution.

In order to prove the validity of the choice of Equation A-3 to give a realization of the clutter video voltage it is convenient to calculate the discrete autocorrelation function. Under the ergodic hypothesis, ensemble averages or expectations of random fields may be replaced by spatial averages. Thus the clutter autocorrelation function may be written

$$B_c(\zeta) = \langle c(t+\zeta)c^*(t)\rangle$$

$$= \frac{1}{NT} \int_0^{NT} c(t+\zeta)c^*(t)dt \tag{A-6}$$

In the discrete case of interest here

$$B_c(kT) = \frac{1}{NT} \sum_n c(nT+kT)c^*(nT)T \tag{A-7}$$

Now the Fourier transform of c and c* given by combining Equations A-2 and A-3 may be used in Equation A-7 to obtain

$$B_c(kT) = \frac{1}{NT} \sum_n \sum_m \sum_{m'} (NT/2\pi) \left[C(m\Delta\omega)C^*(m'\Delta\omega)\right]^{1/2}$$

$$\times r_m r_{m'} e^{i2\pi m(n+k)/N} e^{-i2\pi m'n/N} \Delta\omega^2 T \tag{A-8}$$

Now

$$\sum_n e^{i2\pi mn/N} e^{-i2\pi m'n/N} = N\delta_{mm'} \tag{A-9}$$

So that Equation A-8 becomes

$$B_C(kT) = \sum_m C(m\Delta\omega)e^{i2\pi mk/N} |r_m|^2 \Delta\omega \qquad (A-10)$$

A comparison of the above equation to the continuous relationship between power spectrum and autocorrelation function as given by

$$B_C(t) = \int_{-\infty}^{\infty} C(\omega)e^{i\omega t}d\omega \qquad (A-11)$$

shows that the power spectrum of the numerically generated clutter voltage is $C(m\Delta\omega)|r_m|^2$. It is apparent that different values of the index m correspond to different radian frequency components of the power spectrum. Since $|r_m|^2$ is the sum of the squares of two Gaussian variates, each of the Fourier components of the power spectrum of an individual clutter realization is a chi-squared variate with two degrees of freedom and a mean value of $C(m\Delta\omega)$. Thus for any given clutter realization, the power spectrum will not, in general, be identical to the desired spectrum. However, the average power spectrum of many such clutter voltage realizations may be obtained by taking the expected value of Equation A-10. Since $\langle|r_m|^2\rangle = 1$

$$AVG[B_C(kT)] = \sum_m C(m\Delta\omega)e^{i2\pi mk/N}\Delta\omega \qquad (A-12)$$

which may be compared to Equation A-11. Therefore the average spectrum obtained from many clutter voltage realizations is the desired power spectrum, $C(m\Delta\omega)$, and Equation A-3 is correct.

50

DISTRIBUTION LIST

DEPARTMENT OF DEFENSE

Assistant to the Secretary of Defense
Atomic Energy
      ATTN: Executive Assistant

Defense Advanced Rsch Proj Agency
      ATTN: GSD, R. Alewene
      ATTN: STO, W. Kurowski

Defense Communications Agency
      ATTN: Code 205
      ATTN: Code 230
      ATTN: J300 for Yen-Sun Fu

Defense Communications Engineer Center
      ATTN: Code R410
      ATTN: Code R123, Tech Library
      ATTN: Code R410, N. Jones

Defense Intelligence Agency
      ATTN: DB, A. Wise
      ATTN: DB-4C
      ATTN: DT-1B
      ATTN: Dir
      ATTN: DC-7B

Defense Nuclear Agency
      ATTN: RAAE, P. Lunn
      ATTN: NATD
      ATTN: STNA
      ATTN: RAEE
      ATTN: NAFD
      ATTN: K. Schwartz
3 cy ATTN: RAAE
4 cy ATTN: STTI/CA

Defense Technical Information Center
12 cy ATTN: DD

Dep Under Secretary of Defense
Comm, Cmd, Cont & Intell
      ATTN: Dir of Intelligence Sys

Field Command, DNA, Det 1
Lawrence Livermore National Lab
      ATTN: FC-1

Field Command
Defense Nuclear Agency
      ATTN: FCPR
      ATTN: FCTXE
      ATTN: FCTT, W. Summa

Interservice Nuclear Weapons School
      ATTN: TTV

Joint Chiefs of Staff
      ATTN: C3S
      ATTN: C3S Evaluation Office, HDOO

Joint Data System Support Ctr
      ATTN: G510, G. Jones
      ATTN: C-312, R. Mason
      ATTN: C-500
      ATTN: G510, P. Bird

DEPARTMENT OF DEFENSE (Continued)

Joint Strat Tgt Planning Staff
      ATTN: JLK, DNA Rep
      ATTN: JLAA
      ATTN: JPPFD
      ATTN: JPSS
      ATTN: JLKS
      ATTN: JPTM

National Security Agency
      ATTN: W-36, O. Bartlett
      ATTN: B-3, F. Leonard

Under Secy of Def for Rsch & Engrg
      ATTN: Strat & Theater Nuc Frcs, B. Stephan
      ATTN: Strat and Space Sys (OS)

WWMCCS System Engineering Org
      ATTN: J. Hoff

DEPARTMENT OF THE ARMY

Army Logistics Management Ctr
      ATTN: DLSIE

Assist Chief of Staff for Automation & Comm
      ATTN: DAMO-C4, P. Kenny

Atmospheric Sciences Laboratory
US Army Electronics R&D Command
      ATTN: DELAS-EO, F. Niles

BMD Advanced Technology Center
      ATTN: ATC-R, D. Russ
      ATTN: ATC-R, W. Dickinson
      ATTN: ATC-T, M. Capps
      ATTN: ATC-O, W. Davies

BMD Systems Command
      ATTN: BMDSC-HLE, R. Webb
2 cy ATTN: BMDSC-HW

Dep Ch of Staff for Ops & Plans
      ATTN: DAMO-RQC, C2 Div

Harry Diamond Laboratories
      ATTN: DELHD-NW-R, R. Williams
      ATTN: Chief Div 20000

US Army Chemical School
      ATTN: ATZN-CM-CS

US Army Comm-Elec Engrg Instal Agency
      ATTN: CC-CE-TP, W. Nair

US Army Communications Command
      ATTN: CC-OPS-W
      ATTN: CC-OPS-WR, H. Wilson

US Army Communications R&D Command
      ATTN: DRDCO-COM-RY, W. Kesselman

US Army Foreign Science & Tech Ctr
      ATTN: DRXST-SD

DEPARTMENT OF THE ARMY (Continued)

US Army Materiel Dev & Readiness Cmd
    ATTN: DRCLDC, J. Bender

US Army Nuclear & Chemical Agency
    ATTN: Library

US Army Satellite Comm Agency
    ATTN: Document Control

US Army TRADOC Sys Analysis Actvy
    ATTN: ATAA-PL
    ATTN: ATAA-TDC
    ATTN: ATAA-TCC, F. Payan, Jr

US Army White Sands Missile Range
    ATTN: STEWS-TN-N, K. Cummings

USA Missile Command
    ATTN: DRSMI-YSO, J. Gamble

DEPARTMENT OF THE NAVY

Joint Cruise Missiles Project Ofc
    ATTN: JCMG-707

Naval Air Systems Command
    ATTN: PMA 271

Naval Electronic Systems Command
    ATTN: PME 106-4, S. Kearney
    ATTN: Code 501A
    ATTN: PME 117-211, B. Kruger
    ATTN: Code 3101, T. Hughes
    ATTN: PME-106, F. Diederich
    ATTN: PME-117-2013, G. Burnhart
    ATTN: PME 117-20

Naval Intelligence Support Ctr
    ATTN: NISC-50

Naval Ocean Systems Center
    ATTN: Code 532
    ATTN: Code 5322, M. Paulson
    ATTN: Code 5323, J. Ferguson

Naval Research Laboratory
    ATTN: Code 4720, J. Davis
    ATTN: Code 4700, S. Ossakow
    ATTN: Code 4105, E. Szuszewicz
    ATTN: Code 7500, B. Wald
    ATTN: Code 6700
    ATTN: Code 4700
    ATTN: Code 4780
    ATTN: Code 7950, J. Goodman
    ATTN: Code 4187

Naval Space Surveillance System
    ATTN: J. Burton

Naval Surface Weapons Center
    ATTN: Code F31

Naval Telecommunications Command
    ATTN: Code 341

Ofc of the Deputy Chief of Naval Ops
    ATTN: NO 941D
    ATTN: NOP 981N
    ATTN: NOP 654, Strat Eval & Anal Br

DEPARTMENT OF THE NAVY (Continued)

Office of Naval Research
    ATTN: Code 414, G. Joiner
    ATTN: Code 412, W. Condell

Strategic Systems Project Office
    ATTN: NSP-43, Tech Library
    ATTN: NSP-2141
    ATTN: NSP-2722

Theater Nuclear Warfare Proj Office
    ATTN: PM-23, D. Smith

DEPARTMENT OF THE AIR FORCE

Air Force Geophysics Laboratory
    ATTN: LYD, K. Champion
    ATTN: OPR-1
    ATTN: R. Sabcock
    ATTN: CA, A. Stair
    ATTN: OPR, H. Gardiner
    ATTN: PHY, J. Buchau
    ATTN: R. O'Neil

Air Force Satellite Ctrl Facility
Det 3, AWS
    ATTN: WE

Air Force Space Technology Ctr
    ATTN: YH

Air Force Technical Applications Ctr
    ATTN: TN

Air Force Weapons Laboratory
    ATTN: SUL
    ATTN: NTN
    ATTN: NTCA

Air Force Wright Aeronautical Lab/AAAD
    ATTN: W. Hunt
    ATTN: A. Johnson

Air Logistics Command
    ATTN: OO-ALC/MM

Air University Library
    ATTN: AUL-LSE

Assistant Chief of Staff
Studies & Analysis
    ATTN: AF/SASC, C. Rightmeyer

Ballistic Missile Office/DAA
    ATTN: SYC, D. Kwan
    ATTN: ENSN
    ATTN: ENSN, W. Wilson

Deputy Chief of Staff
Research, Development, & Acq
    ATTN: AFRDT
    ATTN: AFRDS, Space Sys & C3 Dir

Deputy Chief of Staff
Plans and Operations
    ATTN: AFXOKD
    ATTN: AFXDT
    ATTN: AFXONS

DEPARTMENT OF THE AIR FORCE (Continued)

Electronic Systems Div
         ATTN: ESD/SCTE, J. Clark

Electronic Systems Division
         ATTN: SCS-2, G. Vinkels
         ATTN: SCS-1E

Foreign Technology Division
         ATTN: TQTD, B. Ballard
         ATTN: NIIS, Library

Rome Air Development Center
         ATTN: OCS, V. Coyne
         ATTN: OCSA, R. Schneible
         ATTN: TSLD

Rome Air Development Center
         ATTN: EEP, J. Rasmussen
         ATTN: EEPS, P. Kossey

Space Command
         ATTN: DC, T. Long
         ATTN: XPSD, J. Hatlelid

Strategic Air Command
         ATTN: ADWA
         ATTN: DCX
         ATTN: XPQ
         ATTN: XPFC
         ATTN: DCZ
         ATTN: NRI/STINFO Library
         ATTN: XPFS

DEPARTMENT OF ENERGY

Department of Energy
GTN
         ATTN: DP-233

OTHER GOVERNMENT AGENCIES

Central Intelligence Agency
         ATTN: OSWR/NED
         ATTN: OSWR/SSD for K. Feuerpfetl

Department of Commerce
National Bureau of Standards
         ATTN: Sec Ofc for R. Moore

Department of Commerce
National Oceanic & Atmospheric Admin
         ATTN: R. Grubb

Institute for Telecommunications Sciences
National Telecommunications & Info Admin
         ATTN: A. Jean
         ATTN: L. Berry
         ATTN: W. Utlaut

Department of State
Office of International Security Policy
Bureau of Politico Military Affairs
         ATTN: PM/STM

NATO

NATO School, SHAPE
         ATTN: US Documents Officer

DEPARTMENT OF ENERGY CONTRACTORS

EG&G, Inc
         ATTN: J. Colvin
         ATTN: D. Wright

University of California
Lawrence Livermore National Lab
         ATTN: L-31, R. Hager
         ATTN: Tech Info Dept Library

Los Alamos National Laboratory
         ATTN: T. Kunkle, ESS-5
         ATTN: D. Simons
         ATTN: MS 664, J. Zinn
         ATTN: MS 670, J. Hopkins
         ATTN: R. Jeffries
         ATTN: J. Wolcott
         ATTN: P. Keaton

Sandia National Laboratories
         ATTN: T. Cook
         ATTN: B. Murphey

Sandia National Laboratories
         ATTN: Org 1250, W. Brown
         ATTN: Org 4231, T. Wright
         ATTN: Space Project Div
         ATTN: D. Thornbrough
         ATTN: Tech Library 3141
         ATTN: D. Dahlgren

DEPARTMENT OF DEFENSE CONTRACTORS

Aerospace Corp
         ATTN: I. Garfunkel
         ATTN: D. Olsen
         ATTN: J. Kluck
         ATTN: D. Whelan
         ATTN: J. Straus
         ATTN: R. Slaughter
         ATTN: K. Cho
         ATTN: V. Josephson
         ATTN: T. Salmi

Aerospace Corp
         ATTN: S. McWaters

Analytical Systems Engineering Corp
         ATTN: Radio Sciences

Analytical Systems Engineering Corp
         ATTN: Security

BDM Corp
         ATTN: L. Jacobs
         ATTN: T. Neighbors

Berkeley Rsch Associates, Inc
         ATTN: S. Brecht
         ATTN: J. Workman
         ATTN: C. Prettie

Boeing Co
         ATTN: G. Hall

BR Communications
         ATTN: J. McLaughlin

University of California at San Diego
    ATTN: H. Booker

Charles Stark Draper Lab, Inc
    ATTN: A. Tetewski
    ATTN: D. Cox
    ATTN: J. Gilmore

Communications Satellite Corp
    ATTN: D. Fang
    ATTN: G. Hyde

Computer Sciences Corp
    ATTN: F. Eisenbarth

Cornell University
    ATTN: D. Farley, Jr
    ATTN: M. Kelly

E-Systems, Inc
    ATTN: R. Berezdivin

Electrospace Systems, Inc
    ATTN: P. Phillips
    ATTN: H. Logston

EOS Technologies, Inc
    ATTN: W. Lelevier
    ATTN: B. Gabbard

General Electric Co
    ATTN: R. Juner
    ATTN: A. Steinmayer
    ATTN: C. Zierdt

General Electric Co
    ATTN: G. Millman

General Research Corp
    ATTN: B. Bennett
    ATTN: R. Rein
    ATTN: R. Williams

GEO Centers, Inc
    ATTN: E. Marram

GTE Communications Products Corp
    ATTN: R. Steinhoff

GTE Communications Products Corp
    ATTN: J. Concordia
    ATTN: I. Kohlberg

Harris Corp
    ATTN: E. Knick

Honeywell, Inc
    ATTN: G. Terry, Avionics Dept
    ATTN: A. Kearns MS924-3

Horizons Technology, Inc
    ATTN: R. Kruger

HSS, Inc
    ATTN: D. Hansen

IBM Corp
    ATTN: H. Ulander

Institute for Defense Analyses
    ATTN: H. Gates
    ATTN: J. Aein
    ATTN: E. Bauer
    ATTN: H. Wolfhard

ITT Corp
    ATTN: Tech Library

ITT Corp
    ATTN: G. Wetmore

JAYCOR
    ATTN: J. Sperling

JAYCOR
    ATTN: H Dickinson

Johns Hopkins University
    ATTN: C. Meng
    ATTN: K. Potocki
    ATTN: J. Phillips
    ATTN: T. Evans
    ATTN: J. Newland
    ATTN: P. Komiske

Kaman Sciences Corp
Systems Directorate
    ATTN: E. Conrad

Kaman Tempo
    ATTN: B. Gambill
    ATTN: DASIAC
    ATTN: W. Schuleter
    ATTN: W. McNamara

Kaman Tempo
    ATTN: DASIAC

Litton Systems, Inc
    ATTN: B. Zimmer

Lockheed Missiles & Space Co, Inc
    ATTN: R. Sears
    ATTN: J. Kumer

Lockheed Missiles & Space Co, Inc
    ATTN: Dept 60-12
2 cy ATTN: D. Churchill

M. I. T. Lincoln Lab
    ATTN: N. Doherty
    ATTN: V. Vitto
    ATTN: D. Towle

M/A Com Linkabit Inc
    ATTN: A. Viterbi
    ATTN: H. Van Trees
    ATTN: I. Jacobs

Magnavox Govt & Indus Electronics Co
    ATTN: G. White

Maxim Technologies, Inc
    ATTN: E. Tsui
    ATTN: J. Marshall
    ATTN: R. Morganstern

McDonnell Douglas Corp
    ATTN: Tech Library Services
    ATTN: R. Halprin
    ATTN: W. Olson

Meteor Communications Corp
    ATTN: R. Leader

Mission Research Corp
    ATTN: R. Bigoni
    ATTN: G. McCartor
    ATTN: F. Guigliano
    ATTN: F. Fajen
    ATTN: D. Knepp
    ATTN: Tech Library
    ATTN: R. Kilb
    ATTN: R. Bogusch
    ATTN: R. Hendrick
    ATTN: S. Gutsche
    ATTN: R. Dana
2 cy ATTN: C. Lauer
5 cy ATTN: Document Control

Mitre Corp
    ATTN: G. Harding
    ATTN: A. Kymmel
    ATTN: MS J104, M. Oresp
    ATTN: C. Callahan

Mitre Corp
    ATTN: W. Hall
    ATTN: J. Wheeler
    ATTN: W. Foster
    ATTN: M. Horrocks

Pacific-Sierra Research Corp
    ATTN: F. Thomas
    ATTN: H. Brode, Chairman SAGE
    ATTN: E. Field, Jr

Pennsylvania State University
    ATTN: Ionospheric Research Lab

Photometrics, Inc
    ATTN: I. Kofsky

Physical Dynamics, Inc
    ATTN: J. Secan
    ATTN: E. Fremouw

Physical Research, Inc
    ATTN: R. Deliberis
    ATTN: J. Devore
    ATTN: T Stephens
    ATTN: J. Thompson

R&D Associates
    ATTN: R. Turco
    ATTN: M. Gantsweg
    ATTN: C. Greifinger
    ATTN: F. Gilmore
    ATTN: H. Ory
    ATTN: G. Steyr
    ATTN: W. Karzas
    ATTN: W. Wright
    ATTN: P. Haas

R&D Associates
    ATTN: B. Yoon

R&D Associates
    ATTN: G. Ganong

RAND Corp
    ATTN: E. Bedrozian
    ATTN: P. Davis
    ATTN: C. Crain

Rand Corp
    ATTN: B. Bennett

Riverside Research Institute
    ATTN: V. Trapani

Rockwell International Corp
    ATTN: R. Buckner

Rockwell International Corp
    ATTN: S. Quilici

Science Applications, Inc
    ATTN: D. Sachs
    ATTN: C. Smith
    ATTN: D. Hamlin
    ATTN: L. Linson
    ATTN: E. Straker

Science Applications, Inc
    ATTN: J. Cockayne

Science Applications, Inc
    ATTN: M. Cross

SRI International
    ATTN: A. Burns
    ATTN: G. Price
    ATTN: R. Tsunoda
    ATTN: J. Vickrey
    ATTN: V. Gonzales
    ATTN: D. Neilson
    ATTN: J. Petrickes
    ATTN: M. Baron
    ATTN: R. Livingston
    ATTN: D. McDaniels
    ATTN: W. Chesnut
    ATTN: G. Smith
    ATTN: C. Rino
    ATTN: W. Jaye
    ATTN: R. Leadabrand

Stewart Radiance Laboratory
    ATTN: J. Ulwick

Swerling, Manasse & Smith, Inc
    ATTN: R. Manasse

Technology International Corp
    ATTN: W. Boquist

Toyon Research Corp
    ATTN: J. Ise
    ATTN: J. Garbarino

Utah State University
    ATTN: A. Steed
    ATTN: D Burt
    ATTN: K. Baker, Dir Atmos & Space Sci
    ATTN: L. Jensen, Elec Eng Dept

Visidyne, Inc
        ATTN: J. Carpenter
        ATTN: W. Reidy
        ATTN: O. Shepard
        ATTN: C. Humphrey

DEPARTMENT OF DEFENSE CONTRACTORS (Continued)

TRW Electronics & Defense Sector
        ATTN: R. Plebuch

Boeing Co
        ATTN: MS 8K-85, Dr S. Tashird
        ATTN: MS/87-63, D. Clauson